Scatter assessment of rotating system vibrations due to uncertain residual unbalances and bearing properties

Rafał Stocki, Rafał Lasota, Piotr Tauzowski, Tomasz Szolc
Institute of Fundamental Technological Research, Polish Academy of Sciences
Pawińskikiego 5B, 02-106 Warsaw, Poland
e-mail: rstocki@ippt.pan.pl

The main objective of the presented study is an evaluation of the effectiveness of various methods for estimating statistics of rotor-shaft vibration responses. The computational effectiveness as well as the accuracy of statistical moment estimation are essential for efficient robust design optimization of the rotor-shaft systems. The compared methods include sampling techniques, the perturbation approach, the dimension reduction method and the polynomial chaos expansion method. For comparison, two problems of the rotor-shaft vibration analysis are considered: a typical single-span rotor-shaft of the eight-stage centrifugal compressor driven by the electric motor and a large multi-bearing rotor-shaft system of the steam turbo-generator. The most important reason for the observed scatter of the rotor-shaft vibration responses is the inherently random nature of residual unbalances as well as stiffness and damping properties of the journal bearings. A proper representation of these uncertain parameters leads to multidimensional stochastic models. It was found that methods that provide a satisfactory balance between the estimation accuracy and computational effectiveness are sampling techniques. On the other hand, methods based on Taylor series expansion in most of the analyzed cases fail to approximate the rotor-shaft response statistics.

Keywords: stochastic moment estimation, Latin hypercube sampling, polynomial chaos expansion, rotor-shaft system, lateral vibration analysis.

1. INTRODUCTION

In exploitation of rotating machines some of the observed phenomena are considered to be particularly undesired from the viewpoint of effectiveness and safety. Excessive stress concentrations and rubbing effects occurring between stators and rotors attached to flexible shafts subjected to lateral vibrations can be given as examples of such a detrimental behavior. The modern, responsible and heavily affected rotating machines must assure possibly high level of reliability, durability and safety in operation. This is why their designs have to be performed very thoroughly in order to obtain relatively small magnitude of unavoidable dynamic excitation, e.g., due to residual unbalance, gas-pressure forces or electromagnetic forces.

While aiming at realistic modeling of rotor-shaft systems the actual stochastic nature of important model parameters should be taken into account. The main objective of the presented study is to investigate methods that allow for efficient scatter estimation of the rotor-shaft vibration responses. The scatter is basically caused by inherently random rotor-shaft residual unbalances and by uncertain journal bearing parameters. Evaluation of mean values as well as variances of the responses of interest allows not only to assess a typical performance of the rotating machine, but also its sensitivity with respect to parameter imperfections. Efficient methods of statistical moments estimation are a crucial component of robust design optimization (RDO) algorithms. For a comprehensive survey of RDO formulations and solution techniques one can reference e.g., [1, 7, 25]. The

goal of the rotor-shaft robust design optimization is to find the optimal design that is not sensitive with respect to parameter imperfections even when the rotor-shaft is subjected to considerable bending or torsional resonant vibrations.

As mentioned, in the presented paper feasibility of various methods to compute statistical moments of the rotor shaft vibration responses is examined. The investigated methods include sampling techniques, i.e., the classical Monte Carlo as well as Latin hypercube sampling, the Taylor series expansion method, the so-called dimension reduction methods proposed by Xu and Rahman [27] and the polynomial chaos expansion (PCE) method [2, 4]. It must be emphasized that problems concerning the propagation of uncertainty in numerical analysis of complex systems have already been addressed by many authors in numerous papers, see, e.g., [5, 6, 11, 20]. However, these issues do not seem to have been investigated for the rotor shaft systems where the stochastic model is typically represented by a big number of random variables describing residual unbalances and bearing properties.

The paper consists of four main sections. In Sec. 2 each of the studied scatter analysis techniques is shortly described. Section 3 introduces the employed hybrid mechanical model of the rotor-shaft system, which thanks to its high computational efficiency is particularly convenient for stochastic analyses. Finally, in Secs. 4 and 5 the effectiveness of the selected methods for statistical moment estimation is compared using two problems of the rotor-shaft vibration analysis. The first example deals with a typical single-span rotor-shaft of the eight-stage centrifugal compressor driven by an electric motor. In the second example a model of a large multi-bearing rotor-shaft system of the steam turbo-generator is considered.

2. STATISTICAL MOMENT ASSESSMENT

It is fairly typical in mechanical and civil engineering that some quantities which describe a structural system and applied loads should be modeled as random variables, $X_1, X_2, \ldots, X_n$. They are called the basic variables and constitute a random vector $\mathbf{X}$ whose samples $\mathbf{x} = [x_1, x_2, \ldots, x_n]^{\mathrm{T}}$ belong to the Euclidean space. In the space $\mathcal{X}$ the probability measure is defined by the joint probability density function (PDF) $f_{\mathbf{X}}(\mathbf{x})$ of the random vector $\mathbf{X}$. Let a random variable Y, e.g. a rotor-shaft vibration response, be a scalar-valued function of the basic variables in the form:

$$Y = h(\mathbf{X}). \tag{1}$$

In the current study we focus on estimating the mean value μ_Y and the variance $\mathbb{Var}(Y) = \sigma_Y^2$ of Y, which are given, respectively, by:

$$\mu_Y = \mathbb{E}[Y] = \int_{-\infty}^{\infty} h(\mathbf{x}) f_{\mathbf{X}}(\mathbf{x}) \, \mathrm{d}\mathbf{x}, \tag{2}$$

$$\sigma_Y^2 = \mathbb{E}[(Y - \mu_Y)^2] = \int_{-\infty}^{\infty} [h(\mathbf{x}) - \mu_Y]^2 f_{\mathbf{X}}(\mathbf{x}) \, \mathrm{d}\mathbf{x}. \tag{3}$$

The following methods for computing the above moments are investigated:

2.1. Simulation methods

Simulations methods employ samples of basic random variables $\mathbf{X}$ to assess the values of μ_Y and σ_Y^2 defined by (2) and (3). The commonly used unbiased estimators are formulated as follows:

$$\mu_Y \approx \overline{Y} = \frac{1}{N} \sum_{i=1}^{N} Y^{(i)} = \frac{1}{N} \sum_{i=1}^{N} h(\mathbf{X}^{(i)}), \tag{4}$$

$$\sigma_Y^2 \approx s^2 = \frac{1}{N-1}\sum_{i=1}^{N}(Y^{(i)} - \overline{Y})^2 = \frac{1}{N-1}\sum_{i=1}^{N}[h(\mathbf{X}^{(i)}) - \overline{Y}]^2. \tag{5}$$

Realizations $\mathbf{x}^{(i)}$, $i = 1, \ldots, N$, of the random vector $\mathbf{X}$ are drawn from the distribution of $\mathbf{X}$. The simulation methods differ mainly by the way the samples are obtained. One may distinguish two major sampling techniques: random sampling (RS) also known as Monte Carlo sampling and descriptive sampling [19]. Under some assumptions, the so-called Latin hypercube sampling (LHS) [14] can be classified as a descriptive sampling technique. In the performed study the efficiency of RS as well as LHS are examined.

2.2. Taylor series expansion method

An alternative method of estimating statistical moments of random functions is based on expanding these functions into Taylor series around the mean values of random variables, see, e.g., [8]. In the expansion the terms of order higher than two are usually neglected and the stochastic description of variables is given only by the vector of mean values and the covariance matrix. Contrary to sampling techniques that reduce to computing the random function values for many realizations of random variables the major element of the Taylor series expansion method is sensitivity analysis, i.e., computing gradients and higher order derivatives of the functions of interest.

It can be shown that in the case of first order expansion the expectation and the variance of the random function $h(\mathbf{X})$ is approximated, respectively, by:

$$\mathbb{E}[h(\mathbf{X})] \approx h(\boldsymbol{\mu}_{\mathbf{X}}), \tag{6}$$

$$\mathbb{V}\mathrm{ar}[h(\mathbf{X})] \approx \nabla h^{\mathrm{T}}(\mathbf{x})\Big|_{\mathbf{x}=\boldsymbol{\mu}_{\mathbf{X}}} \mathbf{C}_{\mathbf{X}} \nabla h(\mathbf{x})\Big|_{\mathbf{x}=\boldsymbol{\mu}_{\mathbf{X}}}, \tag{7}$$

where $\nabla h(\mathbf{x})\big|_{\mathbf{x}=\boldsymbol{\mu}_{\mathbf{X}}}$ is the gradient of function h computed at mean value point $\boldsymbol{\mu}_{\mathbf{X}}$, and $\mathbf{C}_{\mathbf{X}}$ is the covariance matrix of $\mathbf{X}$ with elements $C_{i,j} = \mathbb{C}\mathrm{ov}(X_i, X_j) = \rho(X_i, X_j)\sigma_{X_i}\sigma_{X_j}$, $i, j = 1, \ldots, n$, where $\rho(X_i, X_j)$ is the correlation coefficient.

Keeping the second order terms of the Taylor expansion of $h(\mathbf{X})$ the following expected value approximation is obtained:

$$\mathbb{E}[h(\mathbf{X})] \approx h(\boldsymbol{\mu}_{\mathbf{X}}) + \frac{1}{2}\sum_{i=1}^{n}\sum_{j=1}^{n}\frac{\partial^2 h(\mathbf{x})}{\partial x_i \partial x_j}\Big|_{\mathbf{x}=\boldsymbol{\mu}_{\mathbf{X}}}\rho_{ij}\,\sigma_{X_i}\sigma_{X_j}. \tag{8}$$

The second order expression for variance requires information on third and fourth order central moments of random variables. Unfortunately, in design practice such a detailed stochastic description is often not available; therefore, the first order approximation, Eq. (7), is usually adopted.

2.3. Dimension reduction method

The dimension reduction method (DRM), see [17, 27], is a relatively new technique of evaluating statistical moments of random functions. In recent years a number of papers were published comparing DRM with other methods [6, 11] and evaluating its feasibility for robust design optimization and structural reliability analysis problems [3, 10, 12, 13]. DRM is based on expanding the random function into Taylor series around mean values of random variables. However, contrary to the approach described in Subsec. 2.2, DRM does not require computation of partial derivatives. As it is shown in [27], the method allows for significant reduction of computational cost with respect to full n-dimensional numerical integration of Eqs. (2) and (3).

Using the dimension reduction method, the multivariate function $h(\mathbf{X})$ is approximated by a sum of less dimensional functions depending only on $s < n$ variables with the other variables fixed to their mean values. From the point of view of computational efficiency the two versions of the method are particularly attractive. These are the univariate dimension reduction (UDR) and the bivariate dimension reduction (BDR) methods given, respectively, by the following expressions:

$$\widehat{h}^{(1)}(\mathbf{X}) \equiv \sum_{i=1}^{n} h(\mu_1, \ldots, \mu_{i-1}, X_i, \mu_{i+1}, \ldots, \mu_n) - (n-1)h(\mu_1, \ldots, \mu_n), \tag{9}$$

$$\widehat{h}^{(2)}(\mathbf{X}) \equiv \sum_{i_1 < i_2} h(\mu_1, \ldots, \mu_{i_1-1}, X_{i_1}, \mu_{i_1+1}, \ldots, \mu_{i_2-1}, X_{i_2}, \mu_{i_2+1}, \ldots, \mu_n)$$

$$- (n-2) \sum_{i=1}^{n} h(\mu_1, \ldots, \mu_{i-1}, X_i, \mu_{i+1}, \ldots, \mu_n) + \binom{n-1}{2} h(\mu_1, \ldots, \mu_n), \tag{10}$$

where μ_i is the mean value of random variable X_i. It can be shown, see [27], that in the case of UDR the approximation error is contributed from the interaction effects among variables and in the case of BDR the error includes only contributions of terms of dimensions 'three' and higher. The l-th moment of the random function $h(\mathbf{X})$ is defined as:

$$m_l = \mathbb{E}[h^l(\mathbf{X})] = \int_{\mathbb{R}^n} h^l(\mathbf{x}) f_{\mathbf{X}}(\mathbf{x}) \, \mathrm{d}\mathbf{x}. \tag{11}$$

Introducing the function $z(\mathbf{X}) = h^l(\mathbf{X})$, Eq. (11) can be expressed in an equivalent form:

$$m_l = \mathbb{E}[z(\mathbf{X})] = \int_{\mathbb{R}^n} z(\mathbf{x}) f_{\mathbf{X}}(\mathbf{x}) \, \mathrm{d}\mathbf{x}. \tag{12}$$

Assuming statistical independence of the random variables and using formulae (9) and (10) the univariate and bivariate approximations of the l-th moment are as follows:

$$m_l \approx \mathbb{E}[\widehat{z}^{(1)}(\mathbf{X})] = \sum_{i=1}^{n} \int_{-\infty}^{\infty} z(\mu_1, \ldots, \mu_{i-1}, x_i, \mu_{i+1}, \ldots, \mu_n) f_{X_i}(x_i) \mathrm{d}x_i - (n-1)z(\mu_1, \ldots, \mu_n), \tag{13}$$

$$m_l \approx \mathbb{E}[\widehat{z}^{(2)}(\mathbf{X})] = \sum_{i_1 < i_2} \int_{-\infty}^{\infty} \int_{-\infty}^{\infty} \Big\{ z(\mu_1, \ldots, \mu_{i_1-1}, x_{i_1}, \mu_{i_1+1}, \ldots, \mu_{i_2-1}, x_{i_2}, \mu_{i_2+1}, \ldots, \mu_n)$$

$$\times f_{X_{i_1}}(x_{i_1}) f_{X_{i_2}}(x_{i_2}) \Big\} \mathrm{d}x_{i_1} \mathrm{d}x_{i_2}$$

$$- (n-2) \sum_{i=1}^{n} \int_{-\infty}^{\infty} z(\mu_1, \ldots, \mu_{i-1}, x_i, \mu_{i+1}, \ldots, \mu_n) f_{X_i}(x_i) \mathrm{d}x_i$$

$$+ \frac{(n-1)(n-2)}{2} z(\mu_1, \ldots, \mu_n), \tag{14}$$

where $f_{X_i}(x_i)$ is PDF of the i-th random variable. If the random variables are stochastically dependent, first they should be transformed into the space of independent standard normal variables using the Rosenblatt transformation [18] or when only marginal distributions of variables and the correlation matrix are known by means of an approximate Nataf transformation [15]. Having computed the first moments m_1 and m_2, the mean value and variance of the random function $h(\mathbf{X})$ are given by

$$\mathbb{E}[h(\mathbf{X})] = m_1, \quad \mathbb{V}\mathrm{ar}[h(\mathbf{X})] = m_2 - m_1^2. \tag{15}$$

In order to assess the value of a statistical moment m_l using equations (13) and (14) it is necessary to perform numerical integration of the functions at most one- and two-dimensional, respectively. If the random variables are normally distributed, then Gauss-Hermite quadratures can be used (integration with the weight function e^{-x^2} over the unbounded interval) and in case of uniform distribution Gauss-Legendre quadratures can be directly employed, see [16]. For other probability distribution functions the most efficient integration approach consists in constructing dedicated quadrature rule, where the nodal points and the corresponding weights are selected according to a given PDF taken as the weight function. A description of such a procedure can be found in, e.g., [11, 17, 27].

The dimension reduction methods compared with standard numerical integration scheme offer a significant improvement in terms of computational efficiency, especially for problems with many variables. Assuming r integration points (nodes) for each direction, $nr + 1$ function evaluations are required to assess the value of an integral using the UDR method and $[n(n-1)/2]\,r^2 + nr + 1$ evaluations when using the BDR method. For example, if $n = 10$ and $r = 4$, then with respect to n dimensional numerical integration 1377 and 25575 times less function evaluations are needed to perform integration by BDR and UDR methods, respectively.

It should be stressed that UDR and BDR methods are not the equivalent of the first and second order Taylor expansion methods. They include, respectively, all the univariate and bivariate terms of any order, which is not the case of the methods described in Subsec. 2.2.

2.4. Polynomial chaos expansion method

The presentation of the method closely follows the one given by Blatman and Sudret in [2]. Provided the variable $Y = h(\mathbf{X})$ has a finite variance, it can be expanded onto the basis of so-called "polynomial chaos" (PC) as follows, see [4, 21]:

$$Y = h(\mathbf{X}) = \sum_{\boldsymbol{\alpha} \in \mathbb{N}^n} a_{\boldsymbol{\alpha}} \psi_{\boldsymbol{\alpha}}(\mathbf{X}), \tag{16}$$

where $a_{\boldsymbol{\alpha}}$ are the unknown deterministic coefficients and $\psi_{\boldsymbol{\alpha}}$ are the multivariate polynomials, orthogonal with respect to the joint PDF $f_{\mathbf{X}}(\mathbf{x})$, which reads

$$\mathbb{E}[\psi_{\boldsymbol{\alpha}}(\mathbf{X})\psi_{\boldsymbol{\beta}}(\mathbf{X})] = \delta_{\boldsymbol{\alpha},\boldsymbol{\beta}}, \tag{17}$$

where $\delta_{\boldsymbol{\alpha},\boldsymbol{\beta}} = 1$, if $\boldsymbol{\alpha} = \boldsymbol{\beta}$ and 0 otherwise.

Assuming independence of the random variables X_i, $i = 1, \ldots, n$, the probability density function of the random vector $\mathbf{X}$ can be expressed as a following product of respective PDFs:

$$f_{\mathbf{X}}(\mathbf{x}) = f_{X_1}(x_1)f_{X_2}(x_2)\cdots f_{X_n}(x_n). \tag{18}$$

In the case of correlated variables, they should be first transformed into the space of independent standard Gaussian variables. Taking advantage of the form of Eq. (18), the polynomials $\psi_{\boldsymbol{\alpha}}$ can be then constructed as a product of n univariate orthogonal polynomials

$$\psi_{\boldsymbol{\alpha}}(\mathbf{X}) = H^{(1)}_{\alpha_1}(X_1)H^{(2)}_{\alpha_2}(X_2)\cdots H^{(n)}_{\alpha_n}(X_n). \tag{19}$$

It can be seen that elements of vector indices $\boldsymbol{\alpha} = \{\alpha_1, \alpha_2, \ldots, \alpha_n\}$ of the multivariate orthogonal polynomials $\psi_{\boldsymbol{\alpha}}$ correspond to degrees of univariate polynomials constituting the above product. Denoting by $\mathcal{D}_{X_i}$ the support of the random variable X_i, the orthogonal polynomials $\{H^{(i)}_k, k \geq 0\}$ satisfying

$$\mathbb{E}[H^{(i)}_k(X_i)H^{(i)}_l(X_i)] = \int_{\mathcal{D}_{X_i}} H^{(i)}_k(x)H^{(i)}_l(x)f_{X_i}(x)\mathrm{d}x = \delta_{k,l}, \quad \forall(k, l \in)\mathbb{N}^2, \tag{20}$$

can be computed using standard algorithms [16]. For standard normal variables the polynomials, which are orthogonal with respect to this PDF, are the Hermite polynomials expressed as:

$$
\begin{aligned}
H_0(x) &= 1, \\
H_1(x) &= x, \\
&\vdots \\
H_{k+1}(x) &= xH_k(x) - kH_{k-1}(x).
\end{aligned}
\tag{21}
$$

In practice, for computational efficiency the series in Eq. (16) is truncated after a finite number of terms. Most often, the polynomials, whose degree $|\boldsymbol{\alpha}|$ is higher than a given degree p, are eliminated from the series

$$
Y = h(\mathbf{X}) \approx \sum_{|\boldsymbol{\alpha}| \leq p} a_{\boldsymbol{\alpha}} \psi_{\boldsymbol{\alpha}}(\mathbf{X}),
\tag{22}
$$

where $|\boldsymbol{\alpha}| = \sum\limits_{i=1}^{n} \alpha_i$. The number of $a_{\boldsymbol{\alpha}}$ coefficients that have to be computed is equal to

$$
M = \binom{n+p}{p}.
\tag{23}
$$

It is estimated, see [2], that the PC approximation with $p = 2$ is usually sufficiently accurate for assessing the first two statistical moments of functions of random variables.

The unknown coefficients are computed either by the so-called projection approach or regression approach. Due to the high computational cost of the first approach, especially when dealing with implicit functions of random variables given by numerical models of structural systems, only the regression approach is described below.

The method based on the concept of linear regression consists in fitting an *a priori* assumed response surface (here it is the truncated PC expansion) to the actual functional relationship given only by its values in a sample of experimental points. Eq. (22) can be written in an equivalent matrix form:

$$
h(\mathbf{X}) \approx \mathcal{H}_p(\mathbf{X}) = \sum_{|\boldsymbol{\alpha}| \leq p} a_{\boldsymbol{\alpha}} \psi_{\boldsymbol{\alpha}}(\mathbf{X}) = \mathbf{a}^{\mathrm{T}} \boldsymbol{\psi}(\mathbf{X}),
\tag{24}
$$

where $\mathbf{a}$ is the vector of coefficients $\{a_{\boldsymbol{\alpha}}, 0 \leq |\boldsymbol{\alpha}| \leq p\}$ and $\boldsymbol{\psi}$ gathers the basis polynomials $\{\psi_{\boldsymbol{\alpha}}, 0 \leq |\boldsymbol{\alpha}| \leq p\}$. Based on the results of N numerical experiments $\{\mathbf{x}_i, y_i\}$, $i = 1, \ldots, N$, where $y_i = h(\mathbf{x}_i)$, the coefficients in Eq. (24) are computed by minimizing a norm of residuals $y_i - \mathcal{H}_p(\mathbf{x}_i)$ usually given by:

$$
S(\mathbf{a}) = \sum_{i=1}^{N} \left[h(\mathbf{x}_i) - \mathbf{a}^{\mathrm{T}} \boldsymbol{\psi}(\mathbf{x}_i) \right]^2.
\tag{25}
$$

The solution vector $\widehat{\mathbf{a}}$ is expressed by the well-known formula:

$$
\widehat{\mathbf{a}} = (\boldsymbol{\Psi}^{\mathrm{T}} \boldsymbol{\Psi})^{-1} \boldsymbol{\Psi}^{\mathrm{T}} \mathbf{y},
\tag{26}
$$

where $\mathbf{y} = \{y_1, \ldots, y_N\}$ is the vector of computed function values in the experimental points and the matrix $\boldsymbol{\Psi}_{N \times M}$ has the form:

$$
\boldsymbol{\Psi} = \begin{bmatrix} \psi_{\boldsymbol{\alpha}_1}(\mathbf{x}_1) & \cdots & \psi_{\boldsymbol{\alpha}_M}(\mathbf{x}_1) \\ \vdots & \ddots & \vdots \\ \psi_{\boldsymbol{\alpha}_1}(\mathbf{x}_N) & \cdots & \psi_{\boldsymbol{\alpha}_M}(\mathbf{x}_N) \end{bmatrix}.
\tag{27}
$$

In order to make this problem well-posed the matrix $\mathbf{\Psi}^{\mathrm{T}}\mathbf{\Psi}$ must be well conditioned. It is then necessary that the employed design of experiments contains a sufficient number of points, preferably significantly more than M.

It is easy to verify, see Eq. (23), that the number of coefficients in expansion (22) grows rapidly with the number of variables n and the polynomial degree p. Therefore, in order to reduce the computational burden and to improve the approximation quality of the method, Blatman and Sudret proposed in [2] an adaptive sparse polynomial chaos expansion. In their approach the iterative algorithm allows to eliminate these of the expansion coefficients which are not significant in approximating the function $h(\mathbf{X})$ leading to an optimal polynomial representation. A version of the sparse PC expansion algorithm, implemented here for the purpose of the current study, was used for assessing statistical moments of the rotor-shaft vibration response.

Applying the assumption of the stochastic independence of random variables $\mathbf{X}$ and the orthogonality of base polynomials $\psi_{\boldsymbol{\alpha}}$, see Eqs. (18)–(20), it is easy to show that the mean value and variance of $h(\mathbf{X})$ are given by:

$$\mathbb{E}[h(\mathbf{X})] \approx \mathbb{E}[\mathcal{H}_p(\mathbf{X})] = a_{\mathbf{0}}, \tag{28}$$

$$\mathbb{V}\mathrm{ar}[h(\mathbf{X})] \approx \mathbb{V}\mathrm{ar}[\mathcal{H}_p(\mathbf{X})] = \sum_{0<|\boldsymbol{\alpha}|\leq p} a_{\boldsymbol{\alpha}}^2, \tag{29}$$

so they are immediately available after obtaining the expansion coefficients $\mathbf{a}_{\boldsymbol{\alpha}}$.

3. DESCRIPTION OF THE HYBRID MECHANICAL MODEL OF THE ROTOR-SHAFT SYSTEM

In order to obtain sufficiently reliable results of numerical simulations together with a reasonable computational efficiency, the vibrating rotor-shaft system of a rotor machine is usually modeled by means of the one-dimensional finite elements of the beam-type. Nevertheless, such models are characterized by relatively high number of degrees of freedom in the range between hundreds and even thousands, which may substantially increase the computational cost of sampling methods. Thus, for such large finite-element models proper algorithms reducing number of degrees of freedom have to be employed in order to shorten computer simulation times. One has to remember that such reductions of degrees of freedom are troublesome and they can lead to computational inaccuracies. In order to avoid the abovementioned drawbacks of the finite element approach and to maintain the obvious advantages of this method, in this paper, similarly as in [22–24], the dynamic analysis of the entire rotating system is performed by means of the one-dimensional hybrid structural model consisting of continuous visco-elastic macro-elements and discrete oscillators. This model is employed here for eigenvalue analyses as well as for numerical simulation of lateral vibrations of the rotor-shaft. In the model successive cylindrical segments of the stepped rotor-shaft are substituted by flexurally and torsionally deformable cylindrical macro-elements of continuously distributed inertial-visco-elastic properties. A typical i-th continuous visco-elastic macro-element is presented in Fig. 1.

In this figure, symbols A_i, I_i and I_{0i}, $i = 1, 2, ..., n_e$, denote respectively the cross-sectional area, the diametral and polar geometric moment of inertia and n_e is the total number of macro-elements in the considered hybrid model. The transverse and torsional external loads continuously distributed along the macro-element length l_i are respectively described by the two-argument functions $p_i(x,t)$ and $q_i(x,t)$, where x is the spatial coordinate and t denotes time. With an accuracy that is sufficient for practical purposes, in the proposed hybrid model of the rotor-shaft system, some heavy rotors or coupling disks can be represented by rigid bodies attached to the macro-element extreme cross-sections, as shown in Fig. 1. Here, symbols m_i, J_i and J_{0i} denote respectively the mass and the diametral and polar mass-moments of inertia of this rigid body. Each journal bearing is represented by a dynamic oscillator of two degrees of freedom, where apart from the oil-film interaction also

Fig. 1. Flexurally and torsionally deformable continuous visco-elastic macro-element.

the visco-elastic properties of the bearing housing and foundation are taken into consideration. This bearing model makes possible to represent with a relatively high accuracy kinetostatic and dynamic anisotropic and anti-symmetric properties of the oil-film in the form of constant or variable stiffness and damping coefficients. An example of such a hybrid model of the centrifugal compressor rotor-shaft is presented in Fig. 2. The rotor-shaft is supported on two journal bearings, where the additional support in its mid-span caused by the aero-dynamic cross-coupling effect is also taken into consideration. The complete mathematical formulation and solutions for such hybrid models of the rotor-shaft systems can be found in [22–24].

Fig. 2. Hybrid mechanical model of the compressor rotor-shaft.

For relatively small magnitude of the rotor-shaft system unbalance, e.g., due to residual static and dynamic unbalance of the shaft segments and of the rotor-disks, the coupling effect between the torsional and bending vibrations is usually negligible, which has been demonstrated in [22] and in other publications written by numerous authors. Moreover, since in majority of fluid-flow rotating machinery operating in steady-state conditions the fluctuating components of dynamic torques transmitted by their rotor-shaft systems are very small, in the carried out considerations only flexural excitation causing bending vibrations due to unbalances is going to be taken into account. Thus, simulations of torsional forced vibrations will not be performed.

In the hybrid model flexural motion of cross-sections of each visco-elastic macro-element of the length l_i is governed by the partial differential equations derived using the Timoshenko and Rayleigh rotating beam theory. The motion equation for the visco-elastically supported rotating Rayleigh beam with a circular cross-section has the following form:

$$EI_i \left[1 + e \left(\frac{\partial}{\partial t} - j\Omega(t) \right) \right] \frac{\partial^4 v_i(x,t)}{\partial x^4} - \rho I_i \frac{\partial^4 v_i(x,t)}{\partial x^2 \partial t^2} + j\Omega(t) I_{0i} \frac{\partial^3 v_i(x,t)}{\partial x^2 \partial t}$$

$$+ \rho A_i \frac{\partial^2 v_i(x,t)}{\partial t^2} + c_{si} \frac{\partial v_i(x,t)}{\partial t} + k_{si} v_i(x,t) = p_i(x,t), \qquad (30)$$

where $v_i(x,t) = u_i(x,t) + jw_i(x,t)$, $u_i(x,t)$ is the lateral displacement in the vertical direction and $w_i(x,t)$ the lateral displacement in the horizontal direction, j denotes the imaginary number, $\Omega(t)$ is the current average rotational speed of the shaft, i.e., corresponding to its rigid body motion,

c_{si} and k_{si} denote respectively damping and stiffness coefficients of the shaft uniform support, e denotes the retardation time for beam flexural deformation, ρ is the material density and the index i goes from 1 to n_e denoting the total number of macro-elements in the hybrid model. It is to remark that in the case of the rotating shaft with a circular cross-section the gyroscopic forces mutually couple in (30) bending vibrations in two perpendicular planes, e.g., in the vertical and the horizontal one. The same coupling effect is caused by the material damping term dependent on the rotational speed $\Omega(t)$.

Similarly as in [22–24], mutual connections of the successive macro-elements creating the stepped shaft as well as their interactions with the supports and rigid bodies representing the heavy rotors are described by equations of boundary conditions. These equations contain geometrical conditions of conformity for translational and rotational displacements of extreme cross-sections $x = L_i = l_1 + l_2 + \ldots + l_{i-1}$ of the adjacent $(i-1)$-th and the i-th elastic macro-elements:

$$v_{i-1}(x,t) = v_i(x,t), \qquad \frac{\partial v_{i-1}(x,t)}{\partial x} = \frac{\partial v_i(x,t)}{\partial x}. \tag{31}$$

The second group of boundary conditions are dynamic ones, which in general contain linear, nonlinear and parametric equations of equilibrium for concentrated external forces, static and dynamic unbalance forces and moments, inertial, elastic and external damping forces, support reactions and gyroscopic moments. For example, the dynamic boundary conditions formulated for the rotating Rayleigh beam and describing a simple connection of the mentioned adjacent $(i-1)$-th and the i-th elastic macro-elements have the following form:

$$P_i(t) - m_i \frac{\partial^2 v_i}{\partial t^2} + EI_i \frac{\partial^3 v_i}{\partial x^3} - \rho I_i \frac{\partial^3 v_i}{\partial x \partial t^2} - EI_{i-1} \frac{\partial^3 v_{i-1}}{\partial x^3} + \rho I_{i-1} \frac{\partial^3 v_{i-1}}{\partial x \partial t^2}$$
$$+ j\Omega(t)\rho I_{0i} \frac{\partial^2 v_i}{\partial x \partial t} - j\Omega \rho I_{0,i-1} \frac{\partial^2 v_{i-1}}{\partial x \partial t} = 0, \tag{32}$$

$$- J_i \frac{\partial^3 v_i}{\partial x \partial t^2} + EI_i \frac{\partial^2 v_i}{\partial x^2} - EI_{i-1} \frac{\partial^2 v_{i-1}}{\partial x^2} + j\Omega(t)\rho J_{0i} \frac{\partial^2 v_i}{\partial x \partial t} = 0,$$

where the arguments of functions $v_i(x,t)$ have been omitted for convenience and $P_i(t)$ denotes the transverse external excitation (if any) imposed in this cross-section in the concentrated form.

Shaft interactions with discrete oscillators representing the shaft supports in journal bearings are also described by means of the dynamic boundary conditions. Here, similarly as in [23, 24], such boundary conditions contain anti-symmetrical terms with cross-coupling oil-film stiffness components, which couple shaft bending vibrations in two mutually perpendicular planes. In these equations the stiffness and damping coefficients can be constant or variable, when non-linear properties of the oil-film are taken into consideration.

In order to perform the analysis of natural elastic vibrations, all the forcing and damping terms in the equations of motion (30) and in the boundary conditions have been omitted. Then, upon an application of the variable separation approach to (30) one obtains the following characteristic equation for the considered eigenvalue problem:

$$\mathbf{A}(\omega)\mathbf{B} = \mathbf{0}, \tag{33}$$

where $\mathbf{A}(\omega)$ is the complex characteristic matrix and $\mathbf{B}$ denotes the vector of unknown constant coefficients in the analytical local eigenfuctions defined in [22] for each macro-element in the hybrid model. Thus, the determination of natural frequencies reduces to the search for values of ω, for which the characteristic determinant of matrix $\mathbf{A}$ is equal to zero. The bending global eigenmode functions are then obtained by solving Eq. (33).

The solution for the forced bending vibration analysis has been obtained using the analytical – computational approach demonstrated in detail in [22–24]. Solving the differential eigenvalue

problem (33) for the linearized orthogonal system for each i-th macro-element there is applied the local Fourier solution in the form of following series in orthogonal eigenfunction

$$v_i(x,t) = \sum_{m=1}^{\infty} V_{im}(x)\xi_m(t), \tag{34}$$

where $V_{im}(x) = U_{im}(x) + jW_{im}(x)$, $U_{im}(x)$ is the lateral eigenfunction component in the vertical direction and $W_{im}(x)$ the lateral eigenfunction component in the horizontal direction, j denotes the imaginary number and $\xi_m(t)$ are the unknown scalar time functions which play a role of modal co-ordinates, where $m = 1, 2, \ldots$. According to [22–24], upon a transformation of all excitations acting on the considered system into the orthogonal base of eigenfunctions $V_{im}(x)$, this approach leads to the following set of coupled ordinary differential equations in the modal coordinates $\xi_m(t)$ contained in vector $\mathbf{r(t)}$

$$\mathbf{M_0 \ddot{r}(t) + D(\Omega(t))\dot{r}(t) + K(\Omega(t))r(t) = F(\Omega^2(t), \Theta(t))}, \tag{35}$$

where

$$\mathbf{D(\Omega(t)) = D_0 + D_g(\Omega(t))}, \qquad \mathbf{K(\Omega(t)) = K_0 + K_b + K_d(\Omega(t))}, \qquad \mathbf{\Theta(t)} = \int_0^{\mathbf{t}} \mathbf{\Omega}(\tau)\mathbf{d}\tau.$$

The symbols $\mathbf{M_0}$, $\mathbf{K_0}$ denote, respectively, the constant diagonal modal mass and stiffness matrices, $\mathbf{D_0}$ is the constant symmetrical damping matrix and $\mathbf{D_g(\Omega(t))}$ denotes the skew-symmetrical matrix of gyroscopic effects. Anti-symmetric elastic properties of the journal bearings are described by the skew-symmetrical matrix $\mathbf{K_b}$. Anti-symmetric effects due to Kelvin-Voigt material damping model of the rotating shaft are expressed by the skew-symmetrical matrix $\mathbf{K_d(\Omega(t))}$ and the symbol $\mathbf{F(\Omega^2(t), \Theta(t))}$ denotes the external excitation vector due to the unbalance and gravitational forces. The number of equations (35) corresponds to the number of bending eigenmodes taken into consideration in the range of frequency of interest. These equations are mutually coupled by the out-of-diagonal terms in matrices $\mathbf{D}$ and $\mathbf{K}$ regarded as the response-dependent external excitations expanded in series in the base of orthogonal analytical eigenfunctions. A fast convergence of the applied Fourier solution enables us to reduce the appropriate number of the modal equations to solve in order to obtain a sufficient accuracy of results in the given range of frequency. Here, it is necessary to solve only 10–20 coupled modal equations (35), even in cases of complex mechanical systems, contrary to the classical one-dimensional beam finite element formulation usually leading to large numbers of motion equations corresponding each to more than one hundred or many hundreds degrees of freedom (if the artificial and often error-prone model reduction algorithms are not applied). However, due to the natural, continuous distribution of inertial-visco-elastic properties of the beam macro-elements the hybrid modeling assures at least the same or even better representation of real objects. Its mathematical description is formally strict and demonstrates clearly the qualitative system properties. Thus, the proposed approach is much more convenient for stable and efficient numerical simulations.

In a general case, i.e., for the variable in time shaft average rotational speed $\Omega(t)$ during system start-ups or run-downs, in order to obtain the system's dynamic response equations (35) can be solved by means of a direct integration. However, for the constant shaft rotational speed Ω and for constant stiffness and damping coefficients of the bearing supports equations (35) become a system of linear ordinary differential equations with constant coefficients and harmonic external excitation due to the residual unbalances. Such excitation can be expressed as:

$$\mathbf{F(\Omega^2, \Omega t) = Q + P(\Omega^2)\cos(\Omega t) + R(\Omega^2)\sin(\Omega t)}, \tag{36}$$

where vectors $\mathbf{P(\Omega^2)}$, $\mathbf{R(\Omega^2)}$ contain the modal components of unbalance amplitudes and vector $\mathbf{Q}$ contains the modal components of the rotor-shaft static gravitational load. Then, in order to

obtain the system's steady-state dynamic response, an analytical solution of equations (35) is very convenient. For the mentioned above harmonic excitation (36) the induced steady-state vibrations are also harmonic with the same synchronous circular frequency Ω. Thus, the analytical solutions for the successive modal functions $\xi_m(t)$ contained in vector $\mathbf{r}(\mathbf{t})$ in (35) can be assumed in the following form:

$$\mathbf{r}(\mathbf{t}) = \mathbf{G} + \mathbf{C}\cos(\mathbf{\Omega t}) + \mathbf{S}\sin(\mathbf{\Omega t}), \tag{37}$$

where vectors $\mathbf{C}$, $\mathbf{S}$ contain respectively the modal cosine- and sine-components of forced vibration amplitudes and vector $\mathbf{G}$ contains the modal components of the rotor-shaft static deflection due to the gravitational load. Then, by intoducing (36) and (37) into (35) simplified for $\Omega = \text{const.}$ and mutually grouping together the static terms as well as the dynamic sine and cosine terms, one obtains the following systems of linear algebraic equations:

$$\mathbf{K}(\mathbf{\Omega})\mathbf{G} = \mathbf{Q},$$

$$\left(\mathbf{K}(\mathbf{\Omega}) - \mathbf{\Omega}^2\mathbf{M}_0\right)\mathbf{C} + \mathbf{\Omega D}(\mathbf{\Omega})\mathbf{S} = \mathbf{P}(\mathbf{\Omega}^2), \tag{38}$$

$$\left(\mathbf{K}(\mathbf{\Omega}) - \mathbf{\Omega}^2\mathbf{M}_0\right)\mathbf{S} - \mathbf{\Omega D}(\mathbf{\Omega})\mathbf{C} = \mathbf{R}(\mathbf{\Omega}^2).$$

These equations are very easy to solve with respect of the unknown components of vectors $\mathbf{C}$, $\mathbf{S}$ and $\mathbf{G}$. Then, using (37) the modal co-ordinates $\xi_m(t)$ are determined and by means of the Fourier solution (34) the steady- state system dynamic lateral response is finally obtained.

4. NUMERICAL EXAMPLE: THE CENTRIFUGAL COMPRESSOR ROTOR-SHAFT

4.1. Model description

The hybrid mechanical model of the considered eight-stage centrifugal compressor rotor-shaft is shown in Fig. 2. In order to create an adequate geometrical and mechanical representation, the stepped-rotor shaft of this compressor of the total length 2.8 m and total weight 485 kg has been modeled by means of $n_e = 27$ continuous macro-elements. All geometrical parameters of the successive real rotor-shaft segments together with their material constants as well as the average stiffness and damping coefficients of the oil-film in the bearings of this compressor have been taken from [26].

In the first step of dynamic analysis the eigenvalue problem must be solved in order to obtain fundamental natural frequencies and the corresponding eigenfunctions of bending and torsional vibrations. As it follows from the comparison performed for the constant nominal rotational speed 5626 rpm, the shear effect taken into consideration in the case of Timoshenko's beam theory results in a little bit smaller natural frequency values than these determined by means of Rayleigh's beam model. Here, in the frequency range 0–400 Hz containing the first 10 bending eigenforms, which is the most important from the engineering viewpoint, the respective differences do not exceed 2%. The eigenfunctions corresponding to these natural frequencies and determined using both beam theories respectively overlay each other. According to the above, one can conclude that in this frequency range an application of Rayleigh's rotating beam theory seems to be sufficiently accurate for further simulations of forced vibrations. For the considered compressor rotor-shaft regarded here as dynamically isolated from the driving motor by means of the low-stiffness elastic coupling the torsional eigenvalue problem has been solved using the analogous hybrid (discrete-continuous) model described e.g. in [22]. The obtained in this way the lowest torsional natural frequency values 597.8 and 1212.4 Hz are far away above the fundamental first 10 bending natural frequencies.

Since the dynamic analysis will be carried out not only for steady-state, nominal, out-of-resonance operating conditions, but also for resonances excited during start-ups and run-downs of the compressor, the proper numerical simulation for such operation patterns has to be performed. In order to demonstrate this transient dynamic behavior, an exemplary simulation of the

system switch-on to switch-off operation cycle is briefly described. The cycle consists of the rotor-shaft start-up from its standstill to the nominal over-critical steady-state operation and of the rotor-shaft run-down, i.e., back to the standstill. It is assumed that the considered compressor is driven by an asynchronous motor by means of an elastic coupling, which dynamically isolates the compressor and the motor rotor-shaft from each other. Thus, the carried out study can be focused on vibrations of the compressor rotor-shaft only. Since the first torsional natural frequency of this rotor-shaft is by far higher than its fundamental 10 bending natural frequencies, during the investigated entire dynamic process flexural deformations of the shaft are predominant and the shaft torsional dynamic deformations seem to be negligible. According to the above, the rotor-shaft can be regarded as a torsionally rigid body rotating with a rotational speed gradually varying in time during start-ups and run-downs. However, the shaft bending vibrations induced by the system residual unbalance are taken into consideration. For the assumed residual static unbalances uniformly distributed along each cylindrical rotor-shaft segment the variable external excitation $p_i(x,t)$ in (30) is expressed by means of the following forcing terms:

$$p_i(x,t) = \varepsilon_i \rho A_i \Omega^2(t) \sin(\Theta(t) + \psi_i) \qquad \text{for} \qquad 0 < x < l_i, \qquad i = 1, 2, \ldots, n_e. \tag{39}$$

For the concentrated static unbalances of each rigid body representing rotor-disks the variable external excitation $P_i(t)$ in (32) is described in the analogous way:

$$P_k(t) = \varepsilon_k m_k \Omega^2(t) \sin(\Theta(t) + \psi_k) \qquad \text{for} \qquad x = 0, \qquad k = 1, 2, \ldots, K. \tag{40}$$

In the above formulae ε_i, ε_k denote the proper eccentricities caused by admissible manufacturing errors, ψ_i, ψ_k are the respective phase shift angles of the unbalance circumferential location with respect to the shaft rotation axis, K denotes the total number of rigid disks in the model and the remaining symbols have been already defined in Fig. 1 and in (35). For the assumed hybrid model of the investigated compressor rotor-shaft in the frequency range 0–1000 Hz 14 bending eigenmodes have been considered to solve equations (35) with sufficiently high computational accuracy of the obtained results.

In Fig. 3 there is presented the time history of the average rotational speed $\Omega(t)$ of the rigid-body motion of the compressor rotor-shaft during start-up, steady-state nominal operation and run-down. This time history has been obtained by means of simulation of rigid-body rotational motion of the compressor entire drive system of mass moment of inertia I_z and excited by the asynchronous motor electro-magnetic torque $T_e(\Omega(t), t)$ expressed using proper formulae from [9]. Moreover, the drive system is loaded by the retarding torque $T_r(\Omega^2(t))$ caused by aero-dynamic forces in the compressor stages. Temporary values of these retarding torques are assumed to be proportional to the square of the current shaft average rotational speed $\Omega^2(t)$. Thus, the simulation reduces to numerical integration of the following equation of the system rotational motion:

$$I_z \frac{d\Omega(t)}{dt} = T_e(\Omega(t), t) - T_r(\Omega^2(t)) \tag{41}$$
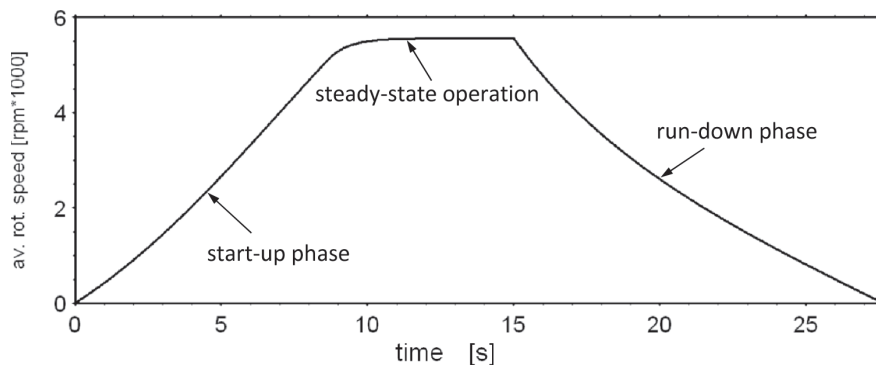

Fig. 3. Time history of the rotor-shaft average rotational speed during start-up, nominal operation and run-down.

performed simultaneously with the numerical simulation of lateral vibrations of the compressor rotor-shaft system. From Fig. 3 it follows that the duration of start-up from the system rest till the nominal operation with the rotational speed 5626 rpm is about 10 s, the nominal operation takes next 5 s and the duration of the run-down is about 13 s. During the start-up and run-down the compressor rotor-shaft passed through the bending vibration resonance zones corresponding to the first two eigenmodes of frequencies respectively equal to 59.4 and 62.6 Hz. These eigenmodes are induced to severe transient resonances by the synchronous excitation due to the unbalances when the rotor-shaft passes the average rotational speed range between 3500 and 3800 rpm, see Fig. 3. The resonances result in a significant increase of bending vibration magnitude, which follows from Fig. 4 demonstrating the system lateral dynamic response corresponding to the variation of the shaft rotational speed during start-up, steady-state nominal operation and run-down shown in Fig. 3. Here, the time history of the lateral displacement at the compressor shaft mid-span is depicted in Fig. 4a and the analogous time history of the transverse force in bearing #2 is shown in Fig. 4b. Here, the lateral displacement has been finally determined using the Fourier solution (34) for the proper cross-section x in the i-th macro-element corresponding to the mentioned compressor rotor-shaft mid-span, where the modal co-ordinates $\xi_i(t)$ are the result of numerical integration of equations (35). The bearing transverse force has been determined in the analogous way in the form of the sum of products of vertical components of the stiffness and damping coefficients multiplied respectively by differences of vertical displacements and velocities between the shaft cross-section corresponding to bearing #2 and the vertical displacement and velocity of the bearing housing, see Fig. 2.

a)

b)
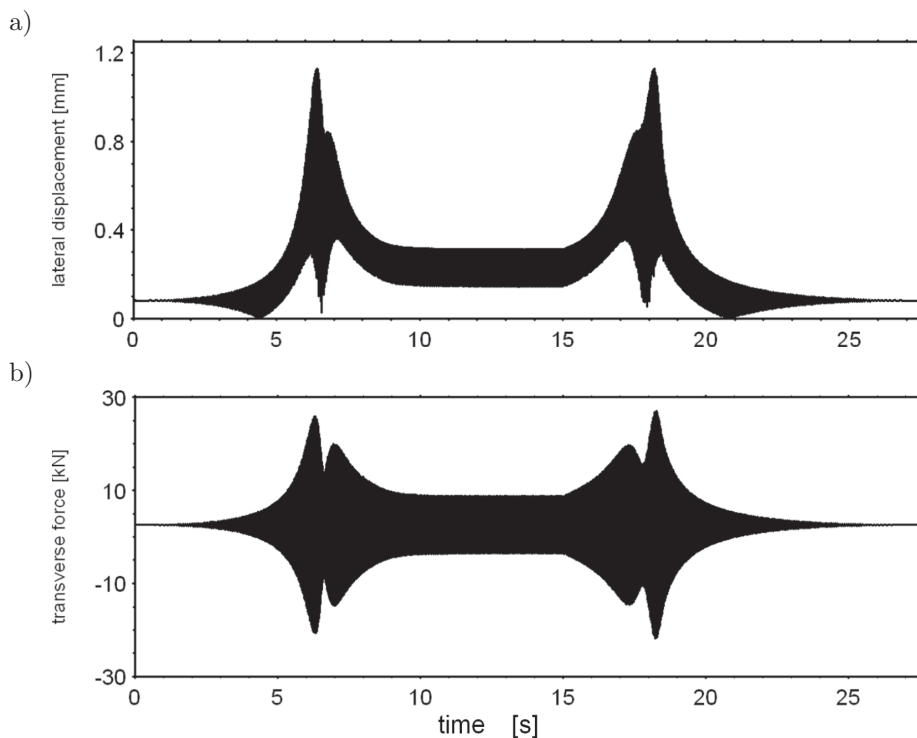
Fig. 4. Time histories of the rotor-shaft response during start-up, nominal operation and run-down:
a) the lateral displacement of the shaft mid-span, b) the transverse force in bearing #2.

As it follows from Figs. 4a and 4b, the passages through these resonances result in very significant increase of dynamic loading of the compressor rotor-shaft in comparison with the steady-state response for the nominal operating conditions at the rotational speed 5626 rpm. Each passage through the resonances causes about 3.6 times greater shaft lateral displacement amplitudes and about 3 times greater amplitudes of the bearing transverse forces. Such an increase of bending vibration magnitude must be associated with a probability of rubbing and with an analogous

increase of the rotor-shaft material stresses, which can cause dangerous material fatigue upon a
given number of routine successive switch-on to switch-off cycles. This obvious fact substantiates
a necessity of analyzing the rotor-shaft vibrations not only for nominal operating conditions, but
first of all, for the transient operation, i.e., for the resonant states. According to the above, apart
from the nominal, steady-state operation at 5626 rpm, which corresponds to synchronous excitation
frequency 93.8 Hz, the dynamical analysis is carried out for resonant working conditions. Then,
the most severe bending vibrations are induced at the synchronous excitation frequency 58.8 Hz
corresponding to the rotor-shaft rotational speed 3525 rpm.

In the example presented below, which is dedicated to estimation of the statistical moments of
the maximal bending vibration amplitude, the vibration response of the rotor shaft system has to
be evaluated for thousands of realizations of the rotor-shaft parameters: unbalance amplitudes and
their phase shift angles, bearing stiffness and damping coefficients etc. For each set of parameters
the analysis is performed for constant values of the shaft rotational speeds respectively 5626 and
3525 rpm. Thus, the computer simulations of forced bending vibrations are reduced solving equa-
tions (35) for $\Omega = $ const. Here, in order to determine system steady-state dynamic responses direct
integration of (35) can be substituted by introducing the analytical solution, which leads to the
straightforward and very effective to solve sets of algebraic equations (38). Similarly, as in the case
of transient bending vibrations excited during start-up and run-down of the compressor, in order to
obtain sufficiently high computational accuracy for steady-state lateral responses the above men-
tioned frequency range 0–1000 Hz containing 14 bending eigenmodes is taken into consideration
for solving equations (38). Here, determination of the rotor-shaft lateral displacements and bearing
vertical force is performed in an identical way as described above for the case of analogous results
obtained by means of integration of equations (35) and depicted in Fig. 4.

4.2. Assessment of statistical moments

The stochastic model of the compressor rotor-shaft contains 64 random variables $\mathbf{X} = \{X_1, \ldots, X_{64}\}$,
cf. Sec. 2, representing uncertain nature of residual unbalances and bearing parameters. The stiffness
as well as damping coefficients of the two journal bearings is represented by 16 normally distributed
variables with the coefficients of variation equal to 10% for the stiffness and 15% for the damping
coefficients. It was assumed that the distribution of residual unbalances of the rotor-shaft segments
(ε_i in Eq. (40)) can be represented by a weighted sum of four principal eigenmodes with the
most probable contribution from the first eigenmode, with the value of the corresponding weight
coefficient up to 0.8, and the contributions from subsequent modes controlled by the maximal values
of their weight coefficients equal to 0.1, 0.08 and 0.02, respectively. Therefore, the weight coefficients
are modeled by uniformly distributed random variables in the ranges $(0, 0.8]$, $(0, 0.1]$, $(0, 0.08]$ and
$(0, 0.02]$. The random magnitude of the unbalances is obtained by setting the maximal value of such
constructed distribution function to be equal to a realization of log-normal random variable with
the expectation 0.15 mm and the standard deviation 0.02 mm. The remaining random parameters
are: 27 uniformly distributed phase shift angles (ψ_i in Eq. (40)) in the range 0–2 π, eight uniformly
distributed rotor-disk unbalances (ε_k in Eq. (40)) in the range 0–1 mm and finally eight uniformly
distributed rotor disk phase shift angles (ψ_k in Eq. (40)) in the range 0–2 π.

The selected method of modeling the unbalances can be justified by a technological process of
the rotor-shaft manufacturing. The predominant unbalance amplitude distribution of the successive
stepped shaft segments according to the first lateral eigenvibration mode is substantiated by the
machining processes typical for the considered rotor-shaft type. Namely, the rotor-shaft usually
clamped at both ends can be forced to bending vibrations by the cutting tool, when an excitation
of the first eigenmode is the most probable and an excitation of the next eigenmodes seems to
be of a secondary importance. The assumed uniform distribution of phase shift angles of these
unbalances follows from the shaft segment-to-segment machining steps usually set as mutually
independent during the entire cutting process. However, the uniform distribution of the gravity

center eccentricities together with their phase shift angles of the rotor-disks can be substantiated by their commonly applied shrink-fit connections with the shaft, which usually requires final balancing of the entire rotor-shaft system upon its 'on-site' assembly.

The rotor-shaft vibrational response $Y(\mathbf{X})$, which mean value and standard deviation are to be estimated, is the maximal vibration amplitude. For the majority of the realizations of the vector $\mathbf{X}$ this maximal lateral rotor-shaft displacement occurs in the mid-span of the rotor-shaft.

In order to establish reference values of the estimated statistics a random sampling with $N = 100\,000$ sample points was performed. The obtained values are $\overline{Y} = 0.4808$ mm and $s = 0.2616$ mm for the mean and standard deviation, respectively, see Eqs. (4) and (5).

In Fig. 5 there is shown a scatter plot prepared for a 5000 point random subset of the $100\,000$ point sample. As can be observed, the majority of realizations of uncertain rotor-shaft parameters lead to moderate displacement magnitudes, however some extreme outlier results may correspond to displacements as high as 1.7 mm. The corresponding histogram presented in Fig. 6 gives some
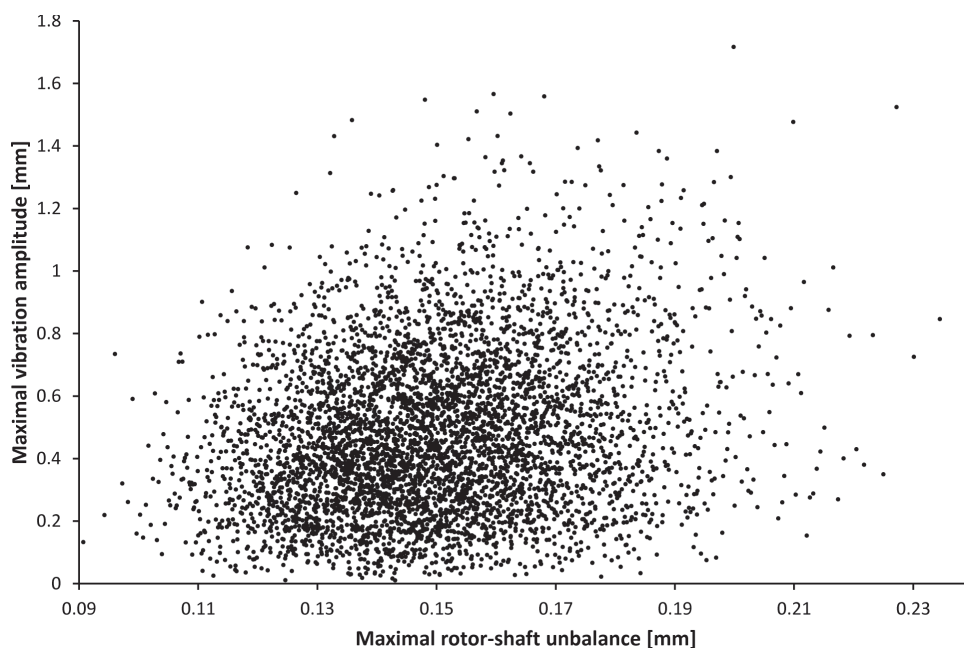
Fig. 5. The compressor rotor shaft example. Scatter of maximal rotor-shaft lateral vibration amplitude.
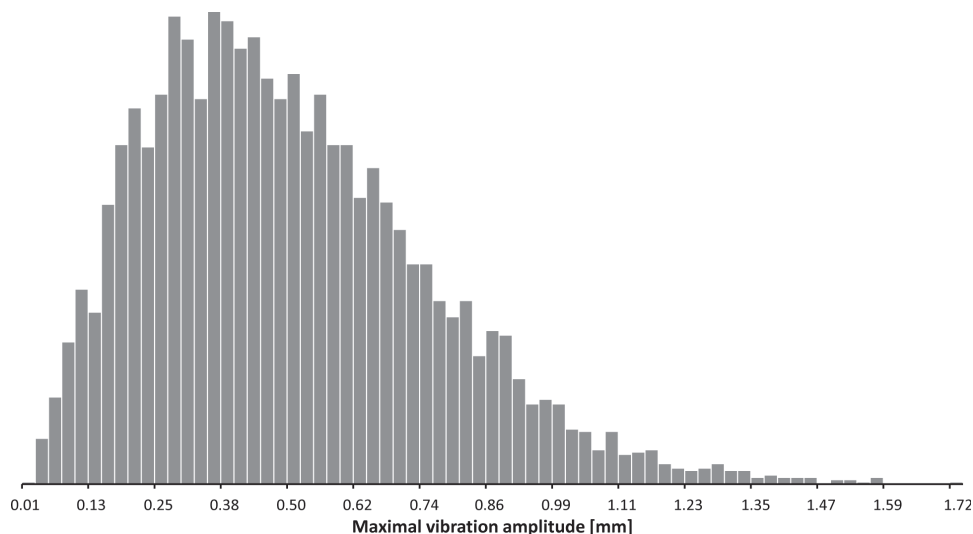
Fig. 6. The compressor rotor shaft example. Histogram of maximal rotor-shaft lateral vibration amplitude.

indication of the kind of probability distribution, the maximal vibration amplitude obeys. The positively skewed histogram can be well approximated by the Weibull probability density functions.

The correlation coefficients between the maximal vibration amplitude and the random variables are illustrated in the form of a bar chart in Fig. 7. By examining their values it could be concluded that there are no random variables significantly correlated with the rotor-shaft response. Lacking statistically dominating relations it is not a straightforward task to eliminate some of the variables from the stochastic model. On the other hand, several random variables seem to influence the output more than the other. These are the maximal rotor-shaft residual unbalance and the direct vertical stiffness and damping coefficients of the journal bearings. Nevertheless, in the performed comparative study the complete set of 64 random variables is taken into account.
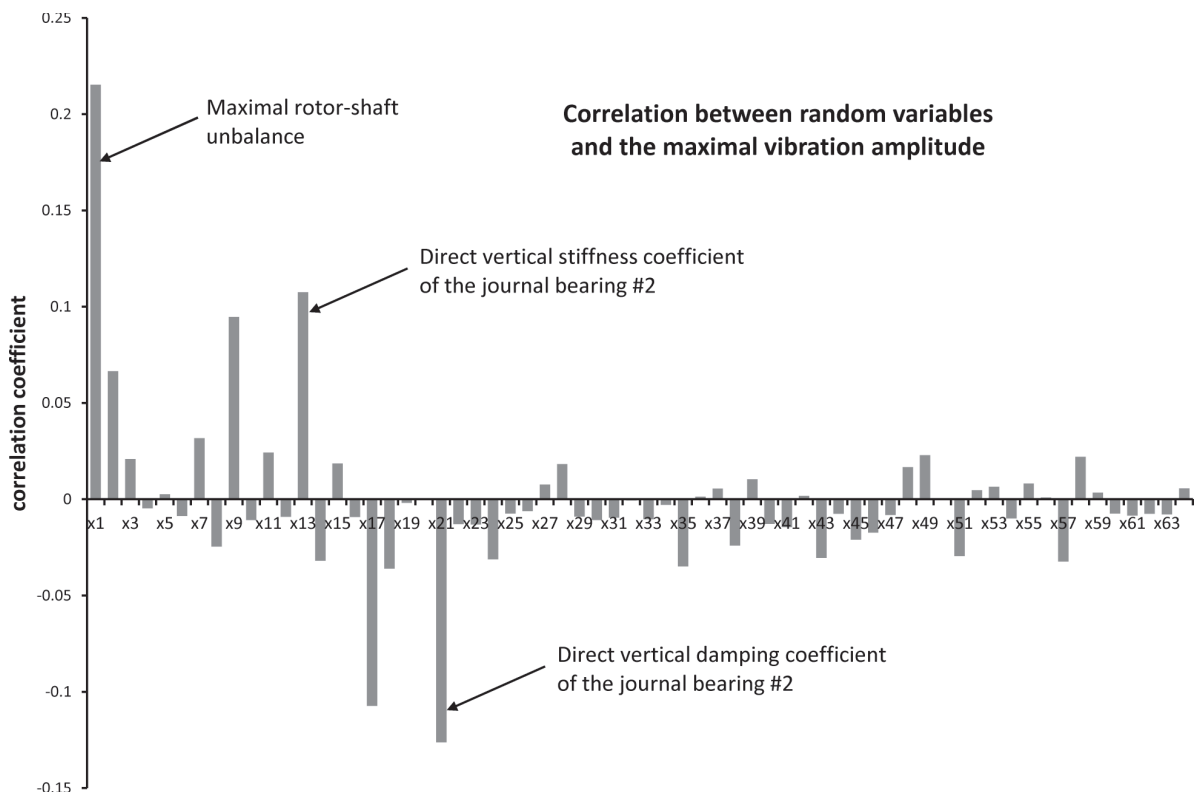
Fig. 7. The compressor rotor shaft example. Correlation coefficients between random variables and the rotor-shaft response.

The methods based on the Taylor series expansion, described in Subsecs. 2.2 and 2.3, entirely failed to estimate the mean and standard deviation of the vibration amplitude. For example, the first order estimation of the mean, see Eq. (6), leads to $\overline{Y} = 2.78$ mm, i.e., to the value many times larger than the reference one. Neither the second order expansion nor the univariate or bivariate reduction approaches provide a substantial improvement of the first order results.

A reason for this unsatisfactory performance may be the way the residual unbalances of the rotor-shaft are modeled. It was assumed that the phase shift angles of the unbalanced circumferential location with respect to the shaft rotation axis are modeled by independent uniformly distributed random variables. Therefore, accounting for the number of rotor-shaft segments, it is extremely unlikely that all the phase shift angles of the rotor-shaft unbalances as well as rotor-disk unbalances take the same values. This, however, is the case for the first order Taylor series expansion approach. All the unbalances are in phase with the phase shift angles equal to the same expected value π. Since the first symmetrical eigenmode determines distribution of residual unbalances, harmonized phase shift angles are the source of significant excitation leading to excessive lateral vibrations. Below,

only the results of sampling methods, see Subsec. 2.1, and sparse PCE technique, see Subsec. 2.4, are presented.

In order to assess the estimation error of the methods employing random sampling and Latin hypercube sampling, the mean value and standard deviation of the rotor-shaft response were computed by RS and LHS for different sample sizes ranging from $N = 120$ to $N = 2400$. For both sampling method and for each N the estimation was performed 300 times using independently generated samples. This allowed to obtain the estimation error statistics, i.e., the mean and standard deviation. The results are shown in Figs. 8 and 9. As it can be seen, in the considered example there is no qualitative difference between RS and LHS and neither of them is visibly superior with respect to the other. It is interesting to observe that even for relatively small samples, i.e. $N = 340 < 6n$, the mean percentage estimation error is less than 3.5%, which seems to be acceptable for the purpose of robust design optimization. According to Eq. (23) assuming the degree of polynomials $p = 2$ and for $n = 64$ random variables, there are 2145 unknown coefficients in the truncated polynomial chaos equation (24). The coefficients have to be determined by the linear regression approach described in Subsec. 2.4. Obviously, the solution (26) depends on the design of experiments used to fit the PC response surface. In the performed study LH based designs of experiments were used for this purpose. In consequence, due to the random nature of such a design, by repeating the analysis for various Latin hypercubes it was possible to obtain estimation error statistics. Two cases were considered: The first one adopting the LH design with $N = 2150$ experimental points, which is slightly more than the number given by Eq. (23), and the second case with $N = 2400$. The employed sparse PCE algorithm, cf. [2], allowed to reduce the number of PC expansion terms to about 690. The reduction leads to an improvement of the linear regression results since a smaller number of coefficients is determined using the same number of experiments. The mean estimation error of the sparse PCE method is compared in Figs. 8 and 9 with the sampling techniques.
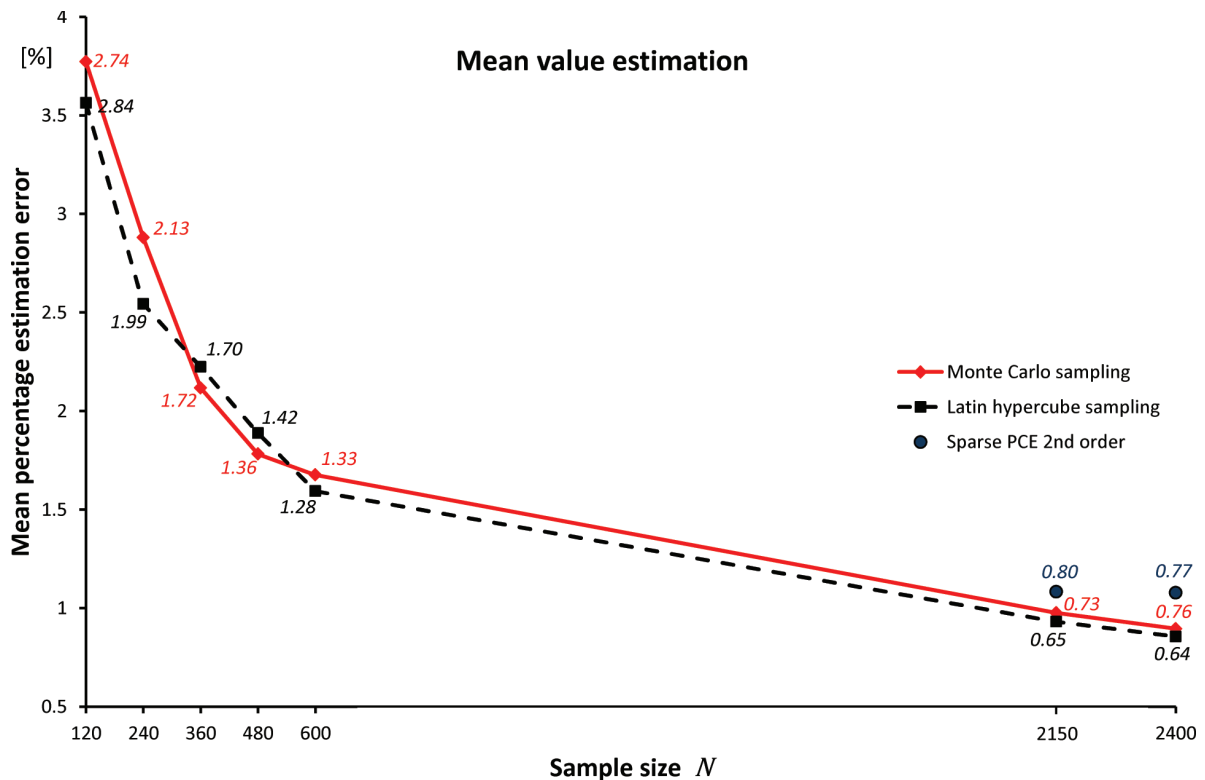

Fig. 8. The compressor rotor shaft example. Mean relative percentage error of the mean value estimation of the maximal rotor-shaft vibration amplitude obtained using RS, LHS and sparse PCE. The graph point labels stand for standard deviations of the errors.
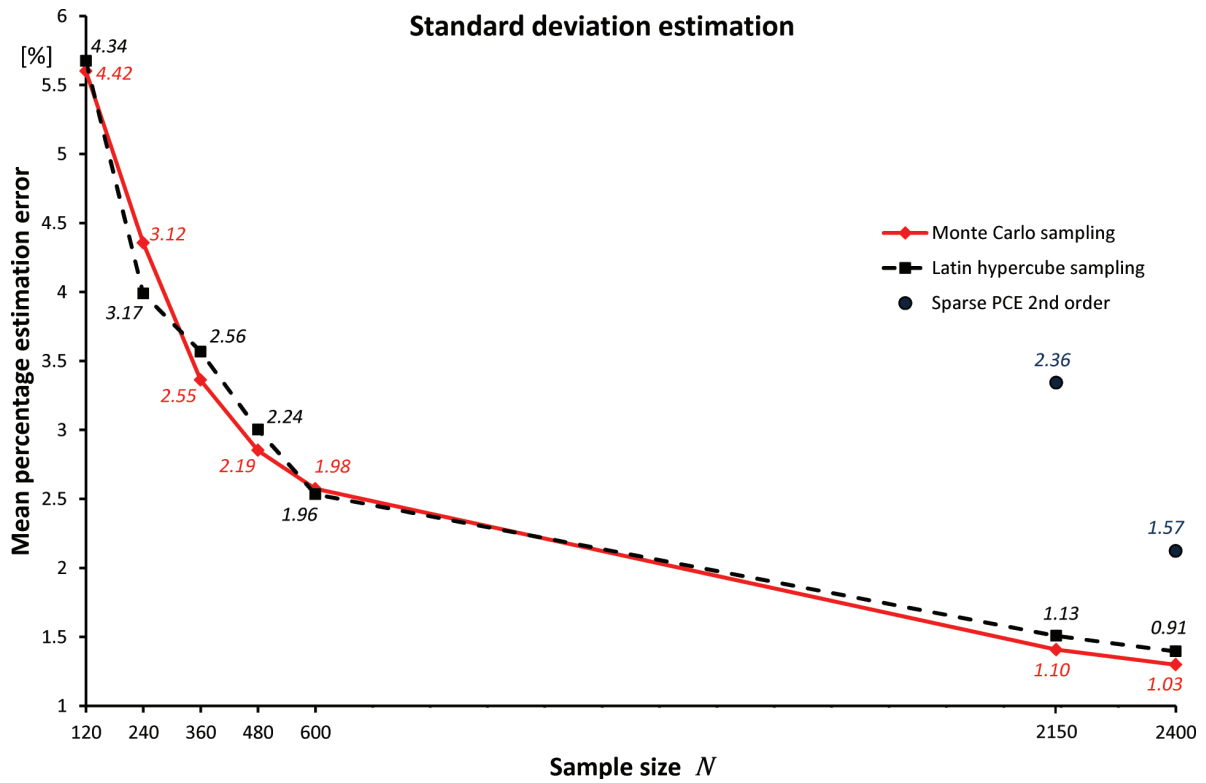
Fig. 9. The compressor rotor shaft example. Mean relative percentage error of the standard deviation estimation of the maximal rotor-shaft vibration amplitude obtained using RS, LHS and sparse PCE. The graph point labels stand for standard deviations of the errors.

In the case of the mean value estimation the error of the PCE method is comparable with MCS and LHS results. On the other hand, the corresponding error of the standard deviation estimation is significantly higher than the one for sampling techniques. Taking into account the reduced number of terms in the PC expansion, the similar results can be obtained for smaller LH design, say for $N \approx 700$. This, however, requires an a priori knowledge of the functional relationship between the random variables and the rotor-shaft response, which is usually not available.

5. NUMERICAL EXAMPLE: THE STEAM TURBO-GENERATOR ROTOR-SHAFT

5.1. Model description

The presented methodology of vibration analysis is applied here in the second numerical example of a rotor-shaft system of the typical 200 MW steam turbo-generator consisting of the single high- (HP), intermediate- (IP) and low-pressure (LP) turbines as well as of the generator-rotor (GEN). The rotor-shaft system is supported by seven journal bearings, as shown in Fig. 10. For the purpose of this study it seems to be sufficient to model the considered stepped-rotor shaft of the total length 25.9 m by means of $n_e = 49$ continuous macro-elements, as an initial approximation
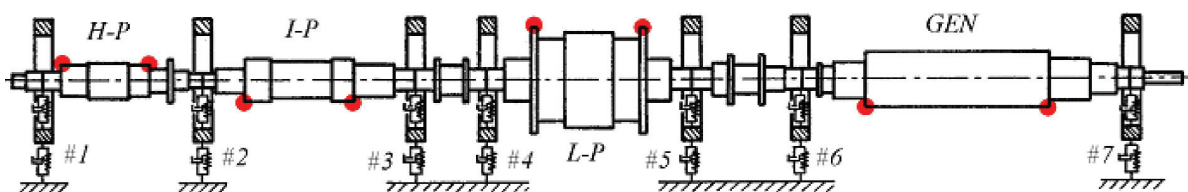
Fig. 10. Hybrid mechanical model of the steam turbo-generator rotor-shaft system.

of its geometry. All geometrical parameters of the successive real rotor-shaft segments as well as their material constants have been determined using the detailed technical documentation of this turbo-generator. The average stiffness and damping coefficients of the oil film in the bearings as well as the equivalent masses and stiffness and damping coefficients of the bearing housings are obtained by means of measurements and identification performed on the real object.

As in the previous numerical example, first the eigenvibration analyses have been performed for the nominal rotational speed of 3000 rpm, using the two abovementioned rotating beam theories. The shear effect taken into consideration in the case of Timoshenko's beam also results in a little bit smaller natural frequency values than these determined by means of Rayleigh's beam model. Here, in the frequency range 0–150 Hz, which is the most important from the engineering viewpoint, the respective differences slightly exceed 3%. The eigenfunctions corresponding to these natural frequencies and determined using both beam theories also respectively overlay each other. Therefore, similarly as in the first example, one can conclude that in this frequency range an application of Rayleigh's rotating beam theory for simulations of forced vibrations seems to be sufficiently accurate, too.

Since a typical high-power turbogenerator is usually put into operation at most few times a year, its start-ups and run-downs are not so frequent exploitation phases as in the case of the above mentioned industrial compressor which can experience successive turn-ons and turn-offs even every day. Moreover, such turbogenerator start-ups and run-downs are always performed satisfying all possible means of security in order to minimize a probability of negative consequences caused by transient vibrations excited during passages through the resonance zones. Therefore, the dynamic and stochastic analyses of the steam turbo-generator rotor-shaft system are going to be carried out only for the steady-state, out-of-resonance operation with the constant nominal rotational speed 3000 rpm corresponding to the excitation of bending vibrations by means of residual unbalances with the synchronous frequency equal to 50 Hz. According to the above, similarly as in the previous "compressor numerical example", computer simulations of forced bending vibrations of the turbo-generator rotor-shaft system are reduced to solving the algebraic equations (38). Here, for the assumed hybrid model of this object in the frequency range of a practical interest 0–500 Hz, 22 bending eigenmodes have been considered to solve (38) with sufficiently high computational accuracy of the obtained results.

5.2. Assessment of statistical moments

The uncertain parameters of the rotor-shaft system are represented by 59 random variables. As in the first numerical example, the stiffness and damping coefficients of seven journal bearings are modeled by normal random variables. However, here the common coefficient of variation is taken equal to 5%. Thus, there are 56 random variables that correspond to the journal bearings, i.e., $7\times(4$ stiffness coefficients $+$ 4 damping coefficients). The remaining three variables account for random values of the residual unbalances.

The rotor-shaft system of the considered turbo-generator consists of the three units described in 5.1, which are independently manufactured and then mutually connected during on-site assembly process of the entire device. Each of them is characterized by a combined cross-sectional structure consisting of the load carrying shaft core and of the strip created by the turbine blade rims or generator windings, respectively, attached along this core by means of a shrink-fit connection. Thus, the residual unbalance distributions of the HP-IP and LP turbines as well as of the generator rotor are in principle not related to the machining process applied as in the case of the centrifugal compressor rotor-shaft, but it is more complicated in character. Taking this into account, it seems to be reasonable to assume that for each given rotor-shaft unit its unbalance is proportional to the successive shaft segment diameters with the common proportionality factor for all segments in the entire unit. For the three rotor-shaft units, this assumption results in three variables that model the uncertainty of residual unbalances. The three proportionality factors are given by realizations

of log-normally distributed random variables. Based on the technical data for the considered turbo-generator rotor-shaft system, the mean values of the 3 uncertain factors were estimated as: $5.6 \cdot 10^{-5}$ for the HP and IP turbines, $2.0 \cdot 10^{-5}$ for the LP turbine and $3.2 \cdot 10^{-6}$ for the generator rotor. The coefficient of variation of these variables was assumed equal to 10%. According to this assumption, each rotor-shaft unit is characterized by the common phase shift angle for all unbalance amplitudes corresponding to successive shaft cylindrical segments. The obtained in this way three phase shift angles for each abovementioned rotor-shaft units are not random, but they are determined from respective identification measurements performed for the real object and assumed equal to zero for the HP-IP turbine, 2.79 rad for the LP turbine and zero for the generator rotor unit.

To get reference values for the mean and standard deviation of maximal rotor-shaft lateral displacement a thorough random sampling with the sample size $N = 100\,000$ was performed. The obtained estimations are $\overline{Y} = 0.0972$ mm and $s = 0.0091$ mm. These values are many times smaller than the corresponding ones from the compressor rotor-shaft example.

When analyzing the simulation results it is interesting to check correlations between the random variables and the considered vibrational response. The values of correlation coefficients are graphically presented in Fig. 11. Contrary to the previous numerical example, here one can easily select variables that strongly influence the value of the vibration amplitude. A random scatter of the values of these variables directly translates into the scatter of the rotor-shaft response. In particular, variable X_{57}, which represents the random factor of residual unbalance magnitude for the HP and IP turbines, is strongly positively correlated with the response. The corresponding correlation coefficient $\rho = 0.84$ indicates that this variable is the major source of the response variance, what can also be observed on the scatter plot in Fig. 12. Thus, a natural choice is to reduce the stochastic description of the rotor shaft by keeping only the variables significantly correlated with the vibrational response. If considering only the three variables marked in Fig. 11, the estimated moments are equal to 0.0975 mm and 0.00838 mm for the mean and standard deviation, respectively. The obtained values provide a very accurate assessment of the moments computed for the full model
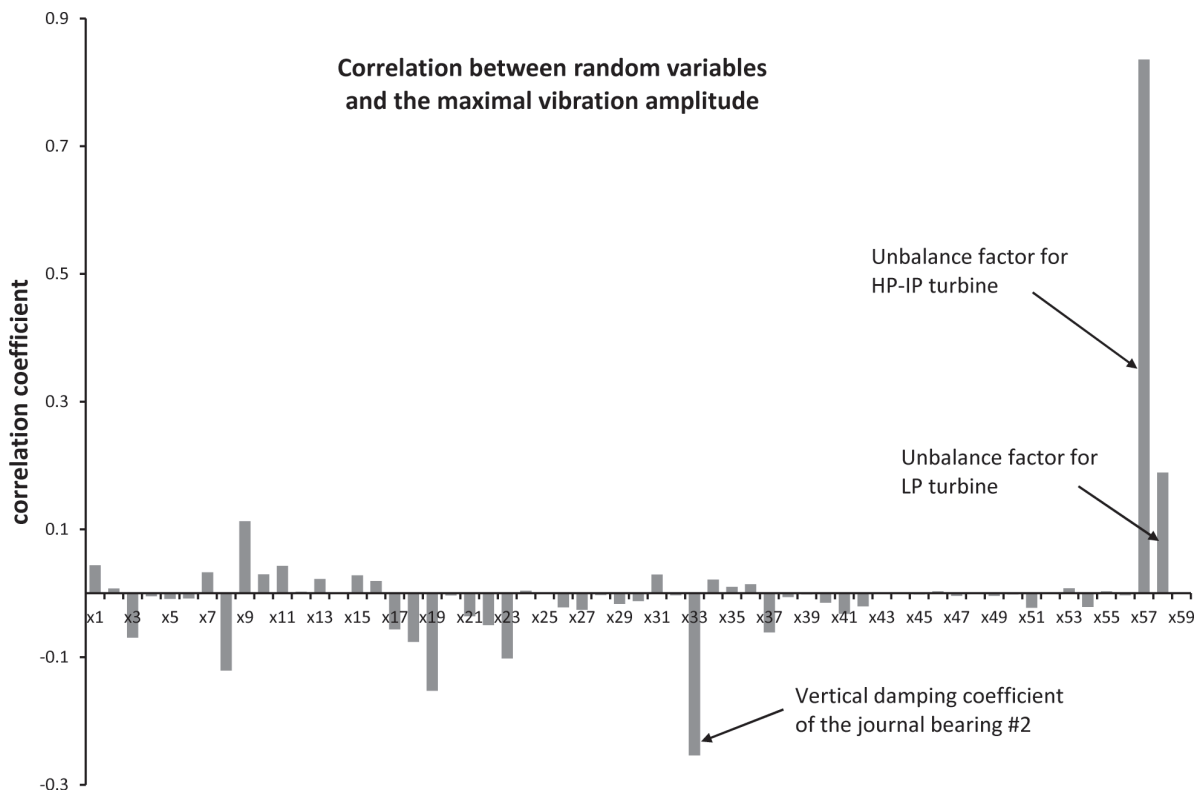

Fig. 11. The turbo-generator rotor shaft example. Correlation coefficients between random variables and the rotor-shaft response.
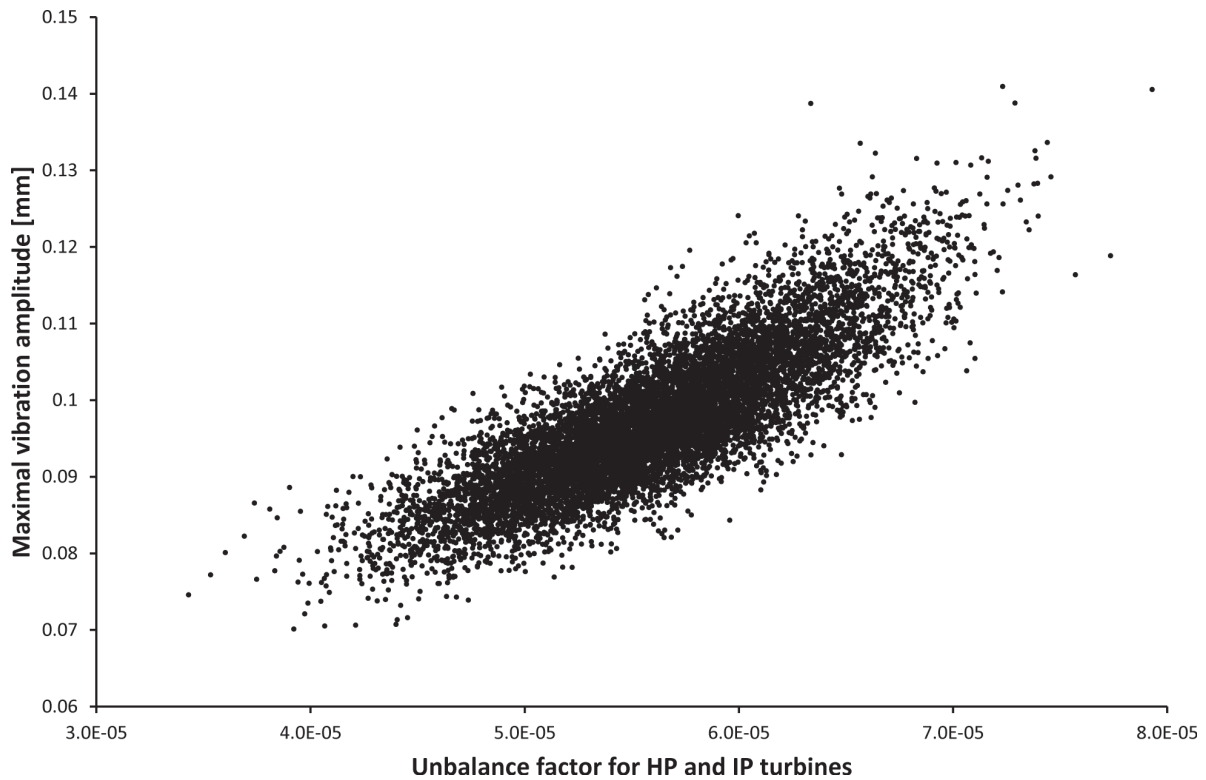
Fig. 12. The turbo-generator rotor shaft example. Scatter of maximal rotor-shaft lateral vibration amplitude.

consisting of 59 variables. If adding two more variables into the reduced model, i.e., variables X_9 and X_{19} corresponding to stiffness coefficients of journal bearings #3 and #5, the estimations of the mean value and standard deviation change to 0.0974 mm and 0.00870 mm, respectively. Since the variance of the reduced model is more than 90% of the variance of the full model, the performance of statistical moment estimation methods was examined for two cases: the full model characterized by 59 variables and the reduced one characterized by 5 variables.

Below, for the complete stochastic model, in Figs. 13 and 14 there are shown the mean percentage estimation errors for moments computed by MCS, LHS and PC expansion methods. The error statistics are based on 300 repetitions of a given method for each value of N. As it can be seen, contrary to the previous numerical example, the Latin hypercube sampling provides the best estimation quality for each sample size.

Even though a very precise estimation of the mean value of the maximal rotor-shaft vibration amplitude can be obtained for relatively small samples, i.e., $N = 120 \approx 2n$, a proper estimation of the standard deviation of this rotor-shaft response requires an application of more sample points, where $N = 360 \div 600$ yields the error of approximately 2%.

The results of the PCE method are very accurate, especially in the case of mean value estimation. Unfortunately for a big number of random variables this approach is rather inefficient due to a size of the necessary design of experiments. When post-processing the sparse PCE results, it turned out that the reduction algorithm allowed to eliminate more than 1000 out of 1830 coefficients from the expansion (24). However, there are still more experimental points than required for sampling methods in order to guarantee an estimation that is accurate enough for the purpose of robust design optimization.

Again, as in the case of the compressor rotor-shaft, the methods based on the Taylor series expansion performed poorly when compared to other techniques. The dimension reduction methods, which have been described in Subsec. 2.3, completely failed to produce results of any relevance to the values of actual statistics. However, contrary to the previous numerical example, here the major
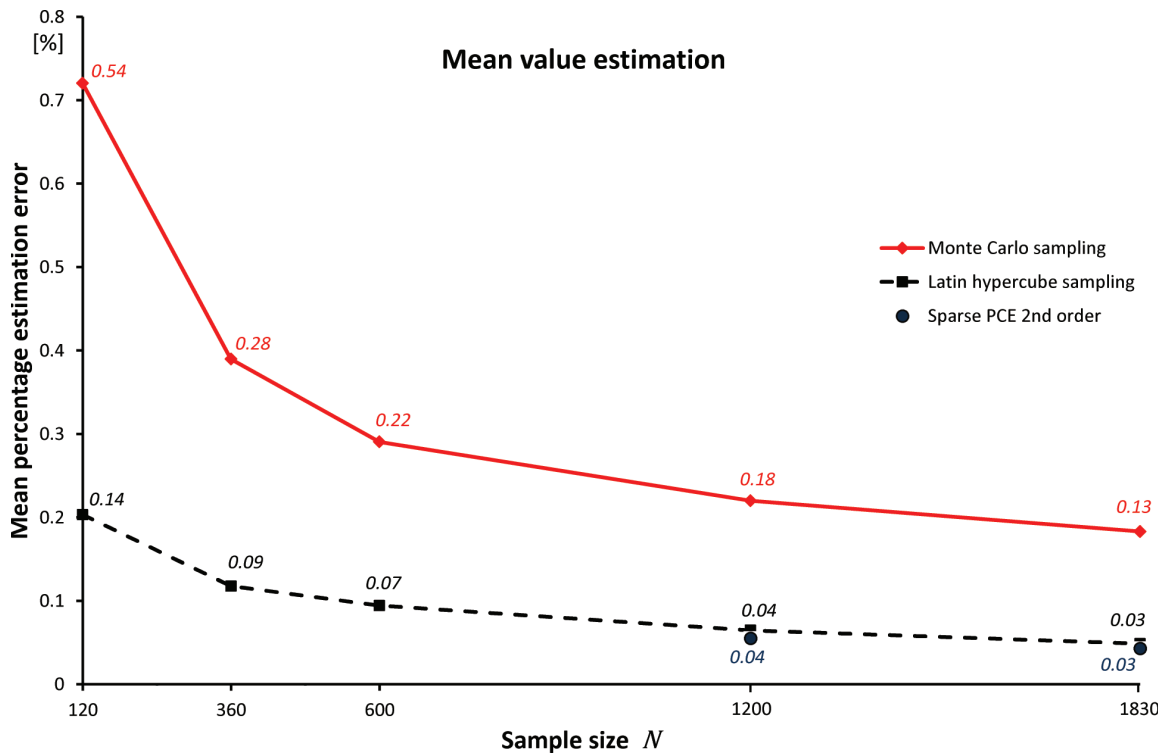
Fig. 13. The turbo-generator rotor shaft example - full model. Mean relative percentage error of the mean value estimation of the maximal rotor-shaft vibration amplitude obtained using RS, LHS and sparse PCE. The graph point labels stand for standard deviations of the errors. The corresponding results for Taylor series expansion methods (Subsec. 2.2): first order – for $N = 61$ the error is 2.4%, second order – for $N = 1830$ the error is 2.3%.
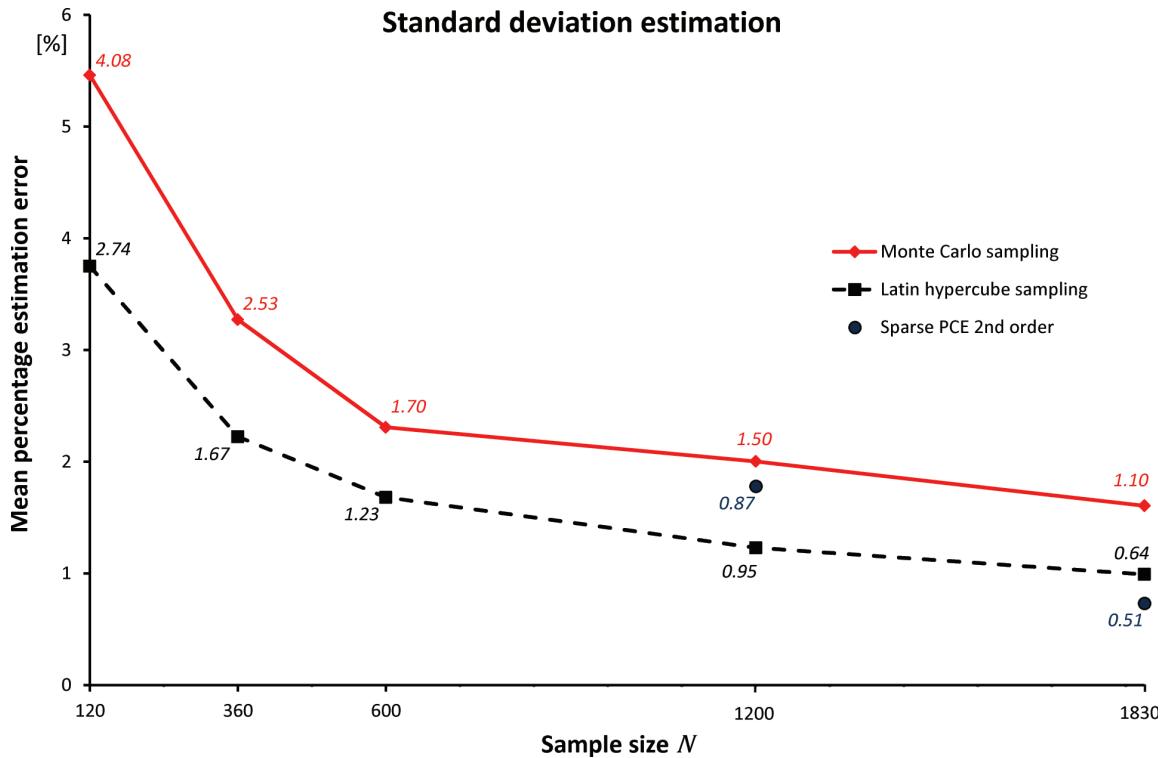

Fig. 14. The turbo-generator rotor shaft example - full model. Mean relative percentage error of the standard deviation estimation of the maximal rotor-shaft vibration amplitude obtained using RS, LHS and sparse PCE. The graph point labels stand for standard deviations of the errors. The corresponding result for Taylor series expansion methods (Subsec. 2.2): first order – for $N = 61$ the error is 12.16%.
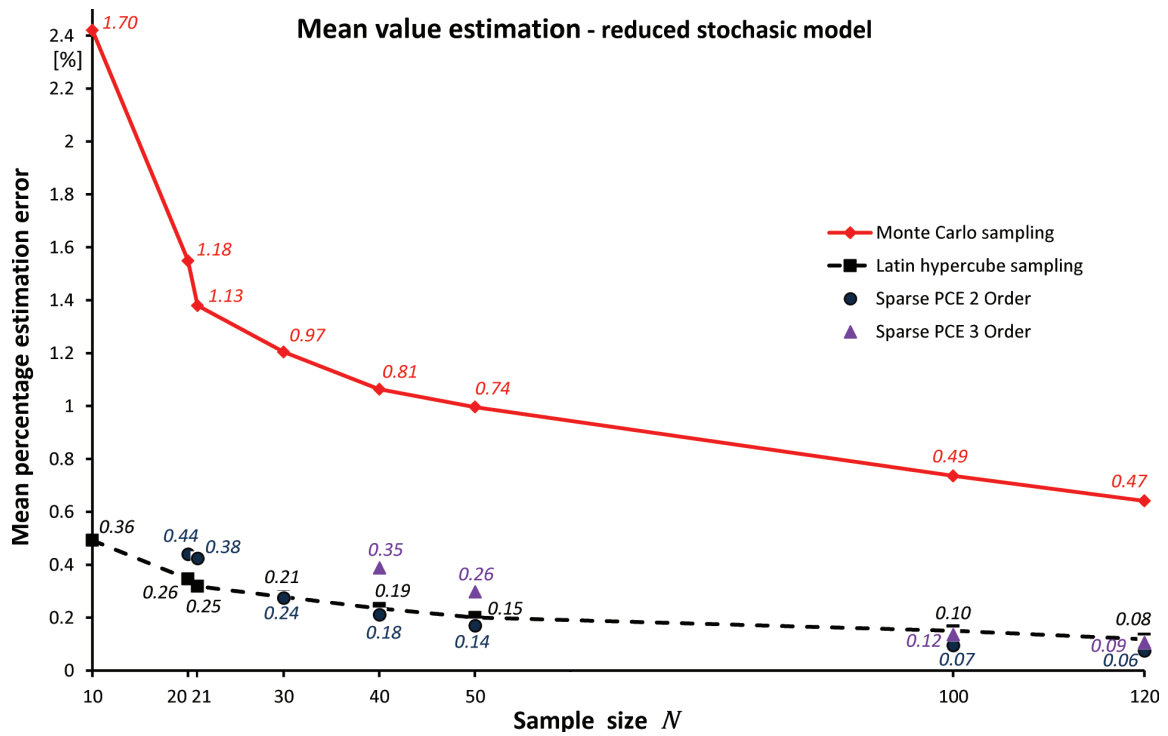
Fig. 15. The turbo-generator rotor shaft example - reduced model. Mean relative percentage error of the mean value estimation of the maximal rotor-shaft vibration amplitude obtained using RS, LHS and sparse PCE. The graph point labels stand for standard deviations of the errors. The corresponding results for Taylor series expansion methods (Subsec. 2.2): first order – for $N = 6$ the error is 2.71%, second order – for $N = 15$ the error is 2.69%. Estimation by UDR (Subsec. 2.3): for $N = 25$ the error is 2.61%.
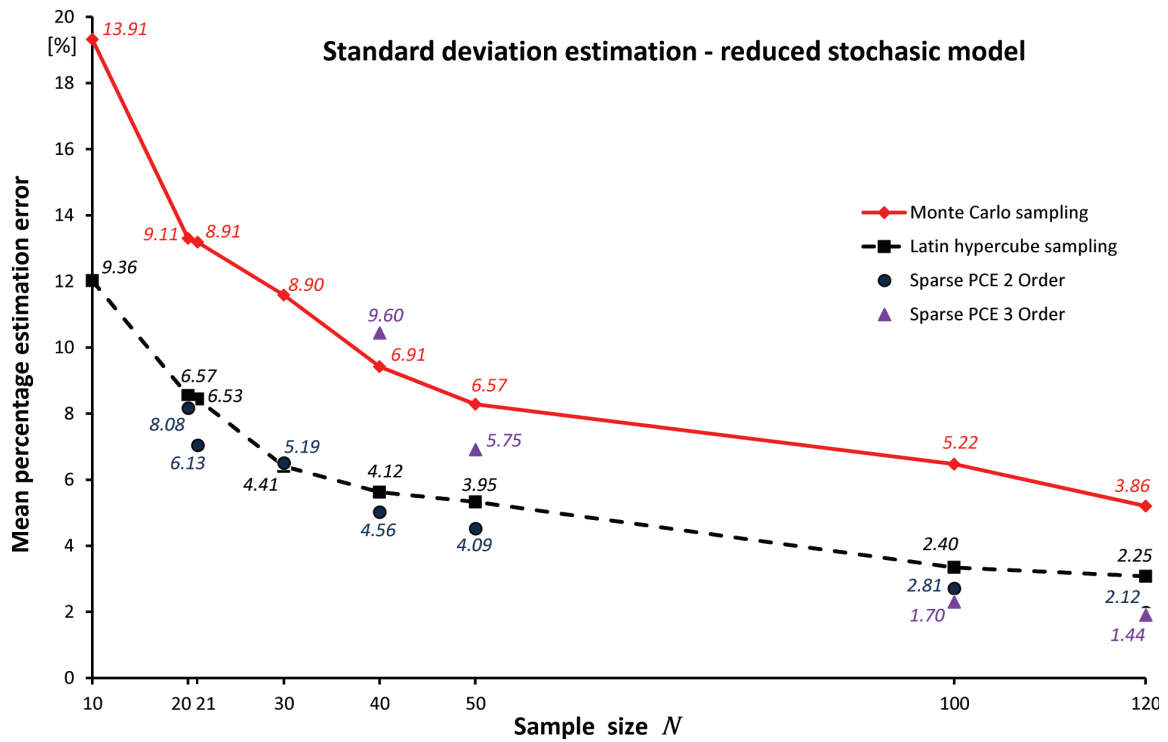
Fig. 16. The turbo-generator rotor shaft example - reduced model. Mean relative percentage error of the standard deviation estimation of the maximal rotor-shaft vibration amplitude obtained using RS, LHS and sparse PCE. The graph point labels stand for standard deviations of the errors.The corresponding result for Taylor series expansion methods (Subsec. 2.2): first order – for $N = 6$ the error is 12.98%. Estimation by UDR (Subsec. 2.3): for $N = 25$ the error is 21.52%.

reason for the observed discrepancies is not connected with the artificial excitation of the rotor-shaft vibrations due to the alignment of unbalance phase shift angles, which has been described in Subsec. 4.2. It seems that for problems with a big number of random variables the values of statistical moments given by Eqs. (13) and (14) may be strongly affected by numerical integration errors, unavoidable when integrating non-polynomial functions using quadrature formulas. The "standard" Taylor series expansion methods described in Subsec. 2.2 yield much better estimations but still they are inferior when compared to simulation methods. The respective results are given in captions of Figs. 13 and 14. In fact, only the first order mean value estimation can be considered as a satisfactory compromise between the estimation accuracy and the computational cost.

The same tests were performed for the reduced stochastic model consisting of 5 random variables. The results are shown in Figs. 15 and 16. They can be examined from two different perspectives. The first one is a comparison of estimation accuracy of the investigated methods for a given sample size. The other perspective is a selection of the sample size that provides sufficient estimation quality in order not to introduce an extensive numerical noise into the objective and constraint functions of the robust design optimization problem.

If we compare the error values computed by RS and LHS techniques obtained for $N = 120$ using the complete and the reduced model, we may notice that the respective values match quite closely. This can be considered as a proof that the adopted reduced model is representative for the complete model and the eliminated variables do not bring much to the response scatter. Therefore, if such a reduction is possible, the non-sampling techniques, such as PCE, which are inefficient for multidimensional problems, may turn out to be competitive with respect to LHS. Especially in estimating the standard deviation, independently of the model used, in order to get a precise estimation, e.g., with the error of about 2%, samples of more than 300 point are necessary for Latin hypercube sampling. On the other hand, if the second order or the third order PCE method is employed, such an estimation accuracy is possible in the case of the reduced model even for $N = 100$.

The results of the Taylor series expansion approach as well as univariate dimension reduction method are given in captions of Figs. 15 and 16. Also in this case they are visibly worse than the estimations provided by other methods.

6. Conclusions

The objective of this study was to examine feasibility of various statistical moment estimation methods for their use in robust design optimization (RDO) of vibrating rotor-shaft systems. The observed scatter of the rotor-shaft vibrational responses is mainly due to the uncertainty of residual unbalances as well as random characteristics of stiffness and damping coefficients of the journal bearings. Since in popular RDO formulations the objective function and design constrains are defined in terms of mean values and variances of selected structural performance functions, the efficiency of statistical moment estimation is crucial for numerical complexity and convergence of the RDO process.

The following methods were compared: the sampling methods (classical Monte Carlo and Latin hypercube sampling), the Taylor series expansion approach, the dimension reduction method and the polynomial chaos expansion method. To evaluate usefulness of a particular method, the mean and standard deviation of the maximal lateral vibration amplitude were estimated for two rotor shafts: the centrifugal compressor rotor-shaft and the turbo-generator rotor-shaft. The vibration analysis was carried out by means of the hybrid structural model consisting of one-dimensional beam-like continuous visco-elastic macro-elements and discrete oscillators. Such a hybrid model proved to be very computationally efficient and reliable, which is of a major importance in the context of stochastic analysis.

A proper representation of uncertain parameters of the rotor-shaft systems may lead to large stochastic models. In the analyzed examples they consisted of 64 and 59 random variables for the

compressor rotor-shaft and the turbo-generator rotor-shaft, respectively. In the second case it was shown that the original model could be reduced to five variables, which are the main sources of the response scatter observed using the full model.

The methods based on the Taylor series expansion performed poorly in both considered cases. For multidimensional problems the dimension reduction technique seems to suffer from using inaccurate numerical integration scheme. On the other hand, the classical Taylor series expansion approach produced acceptable results only for the mean value estimation of the turbo-generator vibrational response. Better estimations were obtained when the reduced stochastic model was employed. Still, they were inferior with respect to the other investigated techniques.

The polynomial chaos expansion method provided stochastic moment assessment of comparable accuracy with the simulation techniques. However, even using the algorithm of eliminating insignificant expansion terms, i.e., sparse PCE, it may be of little practical use for problems involving many (tens, hundreds) random variables. On the other hand, if a reduced stochastic model is available, these methods may turn out to be more efficient than methods based on Latin hypercube sampling.

However, for RDO of the rotor-shaft systems, when the design changes during the optimization process and it is not possible to determine in advance the random variables influencing the response scatter, a "safe" solution seems to be the Latin hypercube sampling. Even for relatively small samples it gives the statistical moment estimation that is sufficient for the purpose of the response surface based RDO.

REFERENCES

[1] H.-G. Beyer and B. Sendhoff. Robust optimization – A comprehensive survey. *Computer Methods in Applied Mechanics and Engineering*, **196**: 3190–3218, 2007.

[2] G. Blatman and B. Sudret. An adaptive algorithm to build up sparse polynomial chaos expansions for stochastic finite element analysis. *Probabilistic Engineering Mechanics*, **25**:183–197, 2010.

[3] J.H. Choi, W.H. Lee, J.J. Park, and B.D. Youn. A study on robust design optimization of layered plate bonding process considering uncertainties. *Structural and Multidisciplinary Optimization*, **35**: 531–540, 2008.

[4] R.G. Ghanem and P.D. Spanos. *Stochastic Finite Elements: A Spectral Approach*. Springer Verlag, 1991.

[5] J.C. Helton and F.J. Davis. Latin hypercube sampling and the propagation of uncertainty in analyses of complex systems. *Reliability Engineering and System Safety*, **81**: 23–69, 2003.

[6] B. Hu and X. Du. Analytical robustness assessment for robust design. *Structural and Multidisciplinary Optimization*, **34**: 123–137, 2007.

[7] Z. Kang. *Robust Design Optimization of Structures under Uncertainty*. Ph.D. Thesis, Institut für Statik und Dynamik der Luft- und Raumfahrkonstruktionen Universität Stuttgart, 2005.

[8] M. Kleiber and T.D. Hien. *The Stochastic Finite Element Method*. Wiley, 1992.

[9] A. Laschet. Simulation von antriebssystemen. *Structural Engineering and Mechanics, Springer-Verlag, Berlin, Heidelberg, London, New-York, Paris, Tokyo*, 1988.

[10] I. Lee, K.K. Choi, L. Du, and D. Gorsich. Dimension reduction method for reliability-based robust design optimization. *Computers and Structures*, **86**: 1550–1562, 2008.

[11] S.H. Lee and W. Chen. A comparative study of uncertainty propagation methods for black-box-type problems. *Structural and Multidisciplinary Optimization*, **37**: 239–253, 2009.

[12] S.H. Lee, W. Chen, and B.M. Kwak. Robust design with arbitrary distributions using gauss-type quadrature formula. *Structural and Multidisciplinary Optimization*, **39**: 227–243, 2009.

[13] S.H. Lee, H.S. Choi, and B.M. Kwak. Multilevel design of experiments for statistical moment and probability calculation. *Structural and Multidisciplinary Optimization*, **37**: 57–70, 2008.

[14] M.D. McKay, R.J. Beckman, and W.J. Conover. A comparison of three methods for selecting values of input variables from a computer code. *Technometrics*, **21**: 239–245, 1979.

[15] A. Nataf. Determination des distribution dont les marges sont donnees. *Comptes Rendus de l'Academie des Sciences*, **225**: 42–43, 1962.

[16] W.H. Press, B.P. Flannery, S.A. Teukolsky, and W.T. Vetterling. *Numerical Recipes in C*. Cambridge University Press, 1988.

[17] S. Rahman and H. Xu. A univariate dimension-reduction method for multi-dimensional integration in stochastic mechanics. *Probabilistic Engineering Mechanics*, **19**: 393–408, 2004.

[18] M. Rosenblatt. Remarks on multivariate transformation. *The Annals of Mathematical Statistics*, **23**: 470–472, 1952.

[19] E. Saliby. Descriptive sampling: an improvement over latin hypercube sampling. In S. Andradóttir, K.J. Healy, D.H. Withers, and B.L. Nelson, editors, *Proceedings of the Winter Simulation Conference*, pages 230–233, 1997.

[20] R. Stocki, P. Tauzowski, and M. Kleiber. Efficient sampling techniques for stochastic simulation of structural systems. *Computer Assisted Mechanics and Engineering Sciences*, **14**: 127–140, 2007.

[21] B. Sudret. Uncertainty propagation and sensitivity analysis in mechanical models – contributions to structural reliability and stochastic spectral methods. *Clermont-Ferrand (France): Habilitation à diriger des recherches. Université Blaise Pascal*, 2007.

[22] T. Szolc. On the discrete-continuous modeling of rotor systems for the analysis of coupled lateral-torsional vibrations. *Int. Journal of Rotating Machinery*, **6**(2): 135–149, 2000.

[23] T. Szolc, P. Tauzowski, J. Knabel, and R. Stocki. Nonlinear and parametric coupled vibrations of the rotor-shaft system as fault identification symptom using stochastic methods. *Nonlinear Dynamics*, **57**: 533–557, 2009.

[24] T. Szolc, P. Tauzowski, R. Stocki, and J. Knabel. Damage identification in vibrating rotor-shaft systems by efficient sampling approach. *Mechanical Systems and Signal Processing*, **23**: 1615–1633, 2009.

[25] Y. Tsompanakis, N.D. Lagaros, and M. Papadrakakis, editors. *Structural Design Optimization Considering Uncertainties*, Structures and Infrastructures Series. Taylor and Francis, 2007.

[26] J.A. Vázques and L.E. Barrett. Modeling of tilting-pad journal bearings with transfer functions. In Agnes Muszyńska, editor, *Proc. 7th Int. Symposium on Transport Phenomena and Dynamics of Rotating Machinery, ISROMAC-7, Honolulu, Hawaii, February (1998)*, volume A, pages 472–481, 1998.

[27] H. Xu and S. Rahman. A generalized dimension-reduction method for multidisciplinary integration in stochastic mechanics. *International Journal for Numerical Methods in Engineering*, **61**: 1992–2019, 2004.